RESEARCH ARTICLE

Atmospheric histories and global emissions of halons H-1211 (CBrClF$_2$), H-1301 (CBrF$_3$), and H-2402 (CBrF$_2$CBrF$_2$)

Martin K. Vollmer[1], Jens Mühle[2], Cathy M. Trudinger[3], Matthew Rigby[4], Stephen A. Montzka[5], Christina M. Harth[2], Benjamin R. Miller[5,6], Stephan Henne[1], Paul B. Krummel[3], Bradley D. Hall[5], Dickon Young[4], Jooil Kim[2], Jgor Arduini[7,8], Angelina Wenger[4], Bo Yao[9], Stefan Reimann[1], Simon O'Doherty[4], Michela Maione[7,8], David M. Etheridge[3], Shanlan Li[10], Daniel P. Verdonik[11], Sunyoung Park[10], Geoff Dutton[5,6], L. Paul Steele[3], Chris R. Lunder[12], Tae Siek Rhee[13], Ove Hermansen[12], Norbert Schmidbauer[12], Ray H. J. Wang[14], Matthias Hill[1], Peter K. Salameh[2], Ray L. Langenfelds[3], Lingxi Zhou[15], Thomas Blunier[16], Jakob Schwander[17], James W. Elkins[5], James H. Butler[5], Peter G. Simmonds[4], Ray F. Weiss[2], Ronald G. Prinn[18], and Paul J. Fraser[3]

[1]Laboratory for Air Pollution and Environmental Technology, Empa, Swiss Federal Laboratories for Materials Science and Technology, Dubendorf, Switzerland, [2]Scripps Institution of Oceanography, University of California, San Diego, La Jolla, California, USA, [3]CSIRO Oceans and Atmosphere, Aspendale, Victoria, Australia, [4]Atmospheric Chemistry Research Group, School of Chemistry, University of Bristol, Bristol, UK, [5]Earth System Research Laboratory, NOAA, Boulder, Colorado, USA, [6]Cooperative Institute for Research in Environmental Sciences, University of Colorado Boulder, Boulder, Colorado, USA, [7]Department of Pure and Applied Sciences, University of Urbino, Urbino, Italy, [8]Institute of Atmospheric Sciences and Climate, Italian National Research Council, Bologna, Italy, [9]Meteorological Observation Centre (MOC), China Meteorological Administration (CMA), Beijing, China, [10]Kyungpook Institute of Oceanography, Kyungpook National University, Daegu, South Korea, [11]JENSEN HUGHES, Baltimore, Maryland, USA, [12]Norwegian Institute for Air Research, Kjeller, Norway, [13]Korea Polar Research Institute, KIOST, Incheon, South Korea, [14]School of Earth and Atmospheric Sciences, Georgia Institute of Technology, Atlanta, Georgia, USA, [15]Chinese Academy of Meteorological Sciences (CAMS), China Meteorological Administration (CMA), Beijing, China, [16]Center for Ice and Climate, Niels Bohr Institute, University of Copenhagen, Copenhagen, Denmark, [17]Climate and Environmental Physics, Physics Institute and Oeschger Centre for Climate Change Research, University of Bern, Bern, Switzerland, [18]Center for Global Change Science, Massachusetts Institute of Technology, Cambridge, Massachusetts, USA

Abstract We report ground-based atmospheric measurements and emission estimates for the halons H-1211 (CBrClF$_2$), H-1301 (CBrF$_3$), and H-2402 (CBrF$_2$CBrF$_2$) from the AGAGE (Advanced Global Atmospheric Gases Experiment) and the National Oceanic and Atmospheric Administration global networks. We also include results from archived air samples in canisters and from polar firn in both hemispheres, thereby deriving an atmospheric record of nearly nine decades (1930s to present). All three halons were absent from the atmosphere until ~1970, when their atmospheric burdens started to increase rapidly. In recent years H-1211 and H-2402 mole fractions have been declining, but H-1301 has continued to grow. High-frequency observations show continuing emissions of H-1211 and H-1301 near most AGAGE sites. For H-2402 the only emissions detected were derived from the region surrounding the Sea of Japan/East Sea. Based on our observations, we derive global emissions using two different inversion approaches. Emissions for H-1211 declined from a peak of 11 kt yr^{-1} (late 1990s) to 3.9 kt yr^{-1} at the end of our record (mean of 2013–2015), for H-1301 from 5.4 kt yr^{-1} (late 1980s) to 1.6 kt yr^{-1}, and for H-2402 from 1.8 kt yr^{-1} (late 1980s) to 0.38 kt yr^{-1}. Yearly summed halon emissions have decreased substantially; nevertheless, since 2000 they have accounted for ~30% of the emissions of all major anthropogenic ozone depletion substances, when weighted by ozone depletion potentials.

1. Introduction

The substantial role of bromine in the depletion of stratospheric ozone has long been recognized, and regulations under the Montreal Protocol have been in place for almost two decades, to reduce the usage and release of brominated compounds to the atmosphere [*Carpenter and Reimann*, 2014]. Here we report on the major halons H-1211 (bromochlorodifluoromethane, CBrClF$_2$), H-1301 (bromotrifluoromethane, CBrF$_3$), and H-2402 (dibromotetrafluoroethane, CBrF$_2$CBrF$_2$). These halons, which evidence suggests are entirely from

anthropogenic activities, have been used as fire suppressants in mobile (mainly H-1211) and stationary (mainly H-1301) fire extinguishers. In contrast, H-2402 was used primarily in the former USSR and was the main halon fire suppressant in that region (UNEP Halon Technical Options Committee, hereafter named the HTOC) [*Halon Technical Options Committee* (*HTOC*), 2011, 2014a; *Kopylov et al.*, 2003]. Due to their widespread use in the past, in particular H-1211 and H-1301, and their decades long atmospheric lifetimes, these halons have accumulated in the atmosphere.

As a consequence of their large ozone depletion potential (ODP), production of these halons has been banned for emissive applications under the regulatory framework of the Montreal Protocol. The ban has been effective since 1994 in non-Article 5 (mainly industrialized) countries and since 2010 in Article 5 (mainly developing) countries. Since use, as such, is not controlled under the Montreal Protocol, active recycling and reuse is ongoing for applications where suitable replacements for these halons have not been identified [*HTOC*, 2011, 2014a]. For example, halons continue to be used in aviation [*HTOC*, 2014b], military equipment, oil and gas pipeline technologies, hospitals, and libraries. Halon production for feedstock applications is exempt from the Montreal Protocol ban. For example, H-1301 is still produced in France and China as feedstock in the manufacture of the pesticide Fipronil [*HTOC*, 2014a]. Also, there are large banks (inventories) of these halons built into equipment. There is a considerable trade of recycled halons to meet needs in existing applications. As a consequence the inventory and trade volumes of the major halons are carefully monitored, and import and export data for recycled halons are collected by the Ozone Secretariat (UNEP).

The three halons discussed here are primarily removed from the atmosphere through photolysis. For H-1301, photolytic removal in the stratosphere is dominant. For H-1211, tropospheric photolysis is the main sink, although photolysis in the stratosphere is also an important sink for this compound. For H-2402, the main sink is in the stratosphere but photolysis in the troposphere is also important (Table 1). *Burkholder et al.* [1991] derived halon atmospheric lifetimes based on laboratory measurements of their ultraviolet (UV) absorption cross sections and their reaction rates with OH. These lifetimes were adopted in several climate reports and ozone depletion assessments [e.g., *Myhre et al.*, 2013; *Montzka et al.*, 2011]. New estimates of halon lifetimes were recently proposed by *Laube et al.* [2013], *Newland et al.* [2013], and by the SPARC (Stratosphere-troposphere Processes And their Role in Climate) project using updated observations (including significant revisions of the H-1211 and H-2402 UV absorption spectra by *Papanastasiou et al.* [2013]), modeling, and other methodologies [*Stratospheric Processes and their Role in Climate* (*SPARC*), 2013]. These new studies have led to significantly different lifetime estimates in the latest WMO/UNEP (World Meteorological Organization/United Nations Environment Programme) Ozone Assessment report [*Carpenter and Reimann*, 2014]. More recently, *Bernard et al.* [2015] revised the UV absorption spectra for H-1301 and they proposed a similar H-1301 atmospheric lifetime as is reported by *SPARC* [2013] but with a significantly reduced uncertainty (Table 1).

Butler et al. [1992] reported on some of the first measurements of H-1211 and H-1301 from the NOAA (National Oceanic and Atmospheric Administration, http://www.esrl.noaa.gov/) network and from oceanic expeditions in the Pacific Ocean. They detected a slowing rate of increase of these halons in the global atmosphere. This was confirmed in 1998 [*Butler et al.*, 1998] when an extended data set became available. In the same paper an inconsistency became apparent between the emissions derived from atmospheric observations and those derived from industry based on production and sales magnitudes (bottom-up inventory based). By 1998, extensive measurements of halons were also made in the lower stratosphere [see *Wamsley et al.*, 1998, and references therein] to get a better understanding of the bromine loading caused by these halons and other bromine-containing compounds. In 1999, *Fraser et al.* [1999] reported on halon measurements from Cape Grim (Tasmania) using the Cape Grim Air Archive (CGAA) samples covering 1978–1999. Using a two-dimensional model, they derived lifetimes for the halons and calculated global emissions. Also, emissions for H-1211 and H-1301 were estimated based on production figures reported by *McCulloch* [1992]. *Reeves et al.* [2005] analyzed the latitudinal distributions of emissions for the halons based on measurements of halons in firn air samples from both hemispheres (Antarctica and Greenland). They concluded that the Northern Hemisphere emissions of H-1211 may have shifted from latitudes near 50°N to near 30°N, reflecting the increased usage by Asian countries. More recently, *Newland et al.* [2013] have reported on updated measurements of the CGAA, which were combined with a two-dimensional atmospheric model to reevaluate the atmospheric lifetimes of the halons and their global emissions.

Table 1. Atmospheric Metrics of H-1211 (CBrClF$_2$), H-1301 (CBrF$_3$), and H-2402 (CBrF$_2$CBrF$_2$)[a]

	H-1211	H-1301	H-2402
ODP, in Montreal Protocol[b]	3.0	10.0	6.0
ODP, semiempirical, WMO[b,c]	7.9	15.9	13.0
ODP, semiempirical, WMO 2014[d]	6.9 (7.7)	15.2 (19.0)	15.7
ODP, semiempirical, *Papanastasiou et al.* [2013]	8.1 (6.2–10.2)	–	18.4 (15.7–21.4)
ODP, semiempirical, *Bernard et al.* [2015]	–	15.7 (15.6–15.9)[e]	–
Stratospheric lifetime (year)			
WMO Ozone Assessment[b]	–	65	–
Newland et al. [2013]	–	–	31 (29–34)
Laube et al. [2013][f]	27 (24–31)	62 (56–69)	–
Laube et al. [1999][g]	36 (32–41)	82 (75–93)	–
SPARC [2013][h]	40.9	79.3	41.3
WMO Ozone Assessment[i]	41	73.5	41
Tropospheric lifetime (year)			
Burkholder et al. [1991]	23	>397	<34
Newland et al. [2013]	25	>10,000	41
SPARC [2013][j]	27.2	3,340	85.5
WMO Ozone Assessment[k]	–	4,490	–
Atmospheric lifetime (year)			
Burkholder et al. [1991]	16	65	<20
WMO Assessment[b]	16[j,k,l]	65[j,k]	20[j,k,l]
Newland et al. [2013]	15 (13–18)	82 (75–93)	17 (16–20)
Papanastasiou et al. [2013][m]	16.4 (12.6–20.6)	–	28.3 (24.2–32.9)
SPARC [2013][c]	16 (10–39)	72 (58–97)	28 (20–45)
WMO Ozone Assessment[i]	16	72	28
Bernard et al. [2015][n]	–	74.6 (73.7–75.5)	–

[a] Abbreviations used in this table are ODP (ozone depletion potential) and WMO (World Meteorological Organization).
[b] WMO Ozone Assessment 2011 [*Montzka et al.*, 2011].
[c] Based on fractional release factors by *Newman et al.* [2007].
[d] WMO Ozone Assessment 2014 [*Harris et al.*, 2014] using the fractional release values by *Newman et al.* [2007] (Values in parenthesis are using fractional release factors by *Laube et al.* [2013]).
[e] These are based on the fractional release factors used in the WMO Assessment 2014 [*Harris et al.*, 2014]. An ODP of 19.7 (19.5–19.9) was calculated using the fractional release factors from *Laube et al.* [2013] and a mean age of air of 3 years. An ODP of 18.6 (18.5–18.6) was calculated based on a two-dimensional model.
[f] Based on a CFC-11 lifetime of 45 years.
[g] Based on a CFC-11 lifetime of 60 years.
[h] Stratosphere-troposphere Processes And their Role in Climate (SPARC), *SPARC* [2013]. Also adopted by the WMO Ozone Assessment 2014 [*Carpenter and Reimann*, 2014]. Numbers in parentheses are "possible ranges." For H-1301, an additional "likely range" of 61–89 is given.
[i] WMO Ozone Assessment 2014 [*Carpenter and Reimann*, 2014].
[j] From previous assessment reports: It includes OH reaction, ocean loss, and stratospheric loss (reactive and photolytic) as appropriate.
[k] Total lifetime taken from Tables 1–4 in *Clerbaux et al.* [2007].
[l] Lifetime is due to a combination of tropospheric and stratospheric photolyses.
[m] *Papanastasiou et al.* [2013] based on revised UV absorption spectra. Numbers in parenthesis are 2σ of uncertainties of the obtained spectra only.
[n] *Bernard et al.* [2015] based on revised UV absorption spectra. Numbers in parenthesis are 2σ of uncertainties of the obtained spectra only.
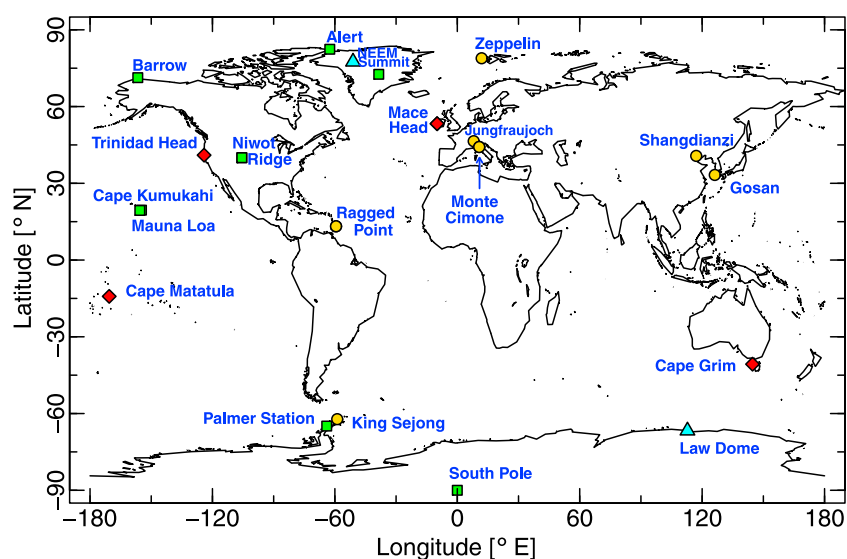
Figure 1. Sampling locations for the halons used in this analysis. Yellow filled circles are sites of AGAGE (Advanced Global Atmospheric Gases Experiment) and related networks, green squares are NOAA (National Oceanic and Atmospheric Administration) sites, and red diamonds are shared sites. The cyan triangles denote the sampling stations for the firn air samples.

Here we report on the measurements of H-1211, H-1301, and H-2402 from the AGAGE (Advanced Global Atmospheric Gases Experiment, https://agage.mit.edu/) and NOAA atmospheric sampling networks, from archived air samples of the CGAA and the Northern Hemisphere, and from a comprehensive set of air samples collected from polar firn in both hemispheres (Figure 1). The data set covers latitudes from 82°N to the South Pole and nearly nine decades from the 1930s to the end of 2015 (Table 2). Our observations are used with the AGAGE 12-box atmospheric model [*Cunnold et al.*, 1983, 1997; *Rigby et al.*, 2013] in two different inversions approaches to derive semihemispheric emissions utilizing updated atmospheric lifetimes. The large geographic and time extent and the comparison of the two networks allow for an improved understanding of the uncertainties in the modeled emissions and atmospheric abundances. We provide an updated intercomparison of our observation-based emission estimates with recently released new HTOC inventory-based emissions allowing a first meaningful H-2402 comparison. For H-2402 we present a Scripps Institution of Oceanography (SIO) primary calibration scale (SIO-14), allowing us for the first time to report the AGAGE data independently and to compare them with other calibration scales. Using a regional model approach for Asia, we identify areas of H-2402 emissions based on the pollution events detected in this region.

2. Materials and Methods

2.1. AGAGE and Affiliated Stations In Situ and Flask Measurements

The AGAGE data used here are from in situ measurements at nine observatories using gas chromatography mass spectrometry (GCMS) technology (see below, Figure 1 and Table 2): The observatories are at Zeppelin (Ny Ålesund, Spitsbergen, Norway), Mace Head (Ireland), Jungfraujoch (Switzerland), Trinidad Head (California, USA), Shangdianzi (China), Gosan (South Korea), Ragged Point (Barbados), Cape Matatula (American Samoa), and Cape Grim (Tasmania, Australia).

The AGAGE in situ measurements are complemented with measurements from affiliated stations (Figure 1), which are also tied into the AGAGE primary calibration scheme to ensure that all measurements are internally consistent with respect to calibration. Here we also include the measurements of H-1211 and H-1301 from the Italian observatory at Monte Cimone, where a different GCMS measurement technique is used [*Maione et al.*, 2013]. We also add flask sample measurements from the South Korean Antarctic station King Sejong, King George Island (South Shetland Islands) from weekly samples collected since 2007 and analyzed at Empa using Medusa-GCMS technology [*Vollmer et al.*, 2011]. Measurements of archived air samples (including firn air samples), as described in more detail below, are also integrated into the AGAGE primary calibration scheme.

Table 2. Station List and Data Used for H-1211 (CBrClF$_2$), H-1301 (CBrF$_3$), and H-2402 (CBrF$_2$CBrF$_2$)[a]

Station	Network/ Institution	Latitude °N	Longitude °E	Altitude[b] (MASL)	Instrument	Data Availability (mm/yyyy) H-1211	H-1301	H-2402
Alert	NOAA	82.4	−62.5	200	GCMS flask	01/1992 to 12/2014	–	02/1995 to 12/2014
Zeppelin	AGAGE	78.9	11.9	475	ADS	01/2001 to 07/2011	01/2001 to 07/2011	–
Zeppelin	AGAGE	78.9	11.9	475	Medusa	09/2010 to 12/2015	09/2010 to 12/2015	09/2010 to 12/2015
NEEM[c]	c	77.5	−51.1	2484	Medusa flask	———————— firn air ————————		
Summit	NOAA	72.6	−38.5	3210	CATS ECD	07/2007 to 12/2014	–	–
Summit	NOAA	72.6	−38.5	3210	GCMS flask	12/2006 to 12/2014	–	–
Barrow	NOAA	71.3	−156.6	11	CATS ECD	06/1998 to 12/2014	–	–
Barrow	NOAA	71.3	−156.6	11	GCMS flask	02/1992 to 12/2014	02/2004 to 12/2014	02/1995 to 12/2014
Mace Head	AGAGE	53.3	−9.9	5	ADS	02/1998 to 03/2005	02/1998 to 03/2005	–
Mace Head	AGAGE	53.3	−9.9	5	Medusa	11/2003 to 12/2015	11/2003 to 12/2015	11/2003 to 12/2015
Mace Head	NOAA	53.3	−9.9	5	GCMS flask	12/1998 to 12/2014	–	–
Jungfraujoch	AGAGE	46.5	8.0	3580	ADS	01/2000 to 04/2008	01/2000 to 04/2008	–
Jungfraujoch	AGAGE	46.5	8.0	3580	Medusa	04/2008 to 12 2015	04/2008 to 12/2015	04/2008 to 12/2015
Monte Cimone	AGAGE	44.2	10.7	2165	GCMS	07/2002 to 12 2015	01/2007 to 12/2015	–
Trinidad Head	AGAGE	41.0	−124.1	107	Medusa	03/2005 to 12/2015	03/2005 to 12/2015	03/2005 to 12/2015
Trinidad Head	NOAA	41.0	−124.1	107	GCMS flask	02/2002 to 12/2014	02/2004 to 12/2014	02/2004 to 12/2014
Shangdianzi	AGAGE	40.7	117.1	293	Medusa	05/2010 to 08/2012	05/2010 to 08/2012	05/2010 to 08/2012
Niwot Ridge	NOAA	40.1	−105.6	3523	CATS ECD	05/2011 to 12/2014	–	–
Niwot Ridge	NOAA	40.1	−105.6	3025	GCMS flask	02/1992 to 12/2014	–	02/1995 to 12/2014
North. Hem. sites	SIO and others	–		–	Medusa flasks	———————— 10/1973 to 12/2013 ————————		
Gosan	AGAGE	33.3	126.2	72	Medusa	11/2007 to 12/2015	11/2007 to 12/2015	11/2007 to 12/2015
Cape Kumukahi	NOAA	19.5	−154.8	3	GCMS flask	11/1995 to 12/2014	07/2004 to 12/2014	11/1995 to 12/2014
Mauna Loa	NOAA	19.5	−155.6	3397	CATS ECD	12/1998 to 12/2014	–	–
Mauna Loa	NOAA	19.5	−155.6	3397	GCMS flask	02/1992 to 12/2014	02/2004 to 12/2014	03/1995 to 12/2014
Ragged Point	AGAGE	13.2	−59.4	15	Medusa	05/2005 to 12/2015	05/2005 to 12/2015	05/2005 to 12/2015
Cape Matatula	AGAGE	−14.2	−170.6	42	Medusa	05/2006 to 12/2015	05/2006 to 12/2015	05/2006 to 12/2015
Cape Matatula	NOAA	−14.2	−170.6	42	CATS ECD	03/1999 to 12/2014	–	–
Cape Matatula	NOAA	−14.2	−170.6	42	GCMS flask	01/1992 to 12/2014	01/2007 to 12/2014	02/1995 to 12/2014
Cape Grim	AGAGE	−40.7	144.7	94	ADS	03/1998 to 02/2005	03/1998 to 02/2005	–
Cape Grim	AGAGE	−40.7	144.7	94	Medusa	01/2004 to 12/2015	01/2004 to 12/2015	01/2004 to 12/2015
Cape Grim	NOAA	−40.7	144.7	94	GCMS flask	02/1992 to 12/2010	02/2004 to 12/2010	02/1995 to 12/2010
Cape Grim	CSIRO/BoM	−40.7	144.7	94	Medusa flasks	———————— 04/1978 to 12/2010 ————————		
King Sejong	KOPRI/Empa	−62.2	−58.8	2	Medusa flasks	02/2007 to 12/2014	02/2007 to 12/2014	02/2007 to 12/2014
Palmer Station	NOAA	−64.9	−64.0	10	GCMS flask	12/1997 to 12/2010	–	04/2009 to 12/2010
Law Dome DSSW20K	d	−66.7	112.5	1200	Medusa flask	———————— firn air ————————		
South Pole	NOAA	−90.0	−4.8	2810	CATS ECD	03/1998 to 12/2010	–	–
South Pole	NOAA	−90.0	−4.8	2810	GCMS flask	01/1992 to 12/2010	11/2004 to 12/2010	10/1995 to 12/2010
South Pole		−90.0	−4.8	2810	Medusa flask	———————— firn air ————————		

[a]Stations are listed in latitudinal order from north to south. Data availability for in situ and flask records with start and end dates. Active NOAA sites are updated to 2014 and active AGAGE sites to 2015. Abbreviations are as follows: AGAGE: Advanced Global Atmospheric Gases Experiment, SIO: Scripps Institution of Oceanography, CSIRO/BoM: CSIRO Oceans and Atmosphere/Australian Bureau of Meteorology, KOPRI: Korea Polar Research Institute, Empa: Swiss Federal Laboratories for Materials Science and Technology, NILU: Norwegian Institute for Air Research.
[b]These are the altitudes of the science buildings. Air intake altitudes at some stations may be higher.
[c]NEEM: North Greenland Eemian Ice Drilling (University of Copenhagen/NEEM consortium/CSIRO).
[d]Law Dome: operated by Australian Antarctic Program/CSIRO. See text for the details on the instrument types NOAA GCMS and ECD, and AGAGE ADS (adsorption-desorption system) and Medusa.

Some of the data from AGAGE and affiliated stations have previously been used in WMO/UNEP Quadrennial Scientific Assessments on Ozone Depletion [e.g., *Carpenter and Reimann*, 2014], by *Maione et al.* [2013] and by *Fraser et al.* [2014].

2.2. AGAGE Measurement Techniques and Instrument Calibrations

Two similar measurement technologies have been used at AGAGE stations over time, both based on GCMS and cryogenic sample preconcentration techniques. The earlier instrument, referred to as the ADS (adsorption-desorption system)-GCMS [*Simmonds et al.*, 1995], was used for several years at the Zeppelin, Mace Head, Jungfraujoch, and Cape Grim stations. These instruments were replaced by a GCMS technique referred to as "Medusa-GCMS" with doubled sampling frequency, differing sample preconcentration methodologies, extended compound selection, and improved measurement precisions [*Miller et al.*, 2008]. The Medusa-GCMS is currently used at all AGAGE stations (Table 2).

For each measurement the analytes from 2 L of air are collected on the sample traps and desorbed onto a single main capillary chromatography column (CP PoraBOND Q, 0.32 mm ID × 25 m, 5 μm, Varian Chrompack, batch-made for AGAGE applications) purged with helium (grade 6.0) that is further purified using a heated getter purifier (He purifier HP2, VICI, USA). The compounds are then detected using a quadrupole mass spectrometer in selected ion mode. Agilent Technology GCs (model 6890N) and MSs are used (initially model 5973, all converted to 5975 over the past years).

For the field Medusa-GCMS instruments, ambient air samples are analyzed every 2 h (c.f. 4 h for the ADS-GCMS) and are bracketed by measurements of quaternary standards to detect and correct for short-term drift in instrument response. The quaternary standards are whole air pressurized into 34 L internally electropolished stainless steel canisters (Essex Industries, USA). They are filled by the groups who are in charge of the respective AGAGE stations using modified oil-free diving compressors (SA-3 and SA-6, RIX Industries, USA) to ∼60 bar (older tanks to ∼30 bar). The exceptions are the sites at Zeppelin and Cape Grim, where the canisters used for quaternary standard purposes are typically filled cryogenically.

The on-site quaternary standards are compared weekly to tertiary standards from the central calibration facility at SIO in order to propagate the primary calibration scales and to characterize any potential long-term drift of the measured compounds in the quaternary standards. The Medusa-GCMS measurement precisions for the three halons for the field instruments are estimated based on the repeated measurements of the quaternary standards. They are typically 0.4–0.8% (1σ) for H-1211 and 1.0–2.5% (1σ) for H-1301 and H-2402.

2.3. Archived Air

Our analysis includes the results from Medusa-GCMS measurements on archived air collected in canisters over the past four decades. We use halon measurements from the CGAA for the Southern Hemisphere, collected since 1978 at the Cape Grim Baseline Air Pollution Station by the Commonwealth Scientific and Industrial Research Organisation (CSIRO) and the Australian Bureau of Meteorology for archival purposes [*Langenfelds et al.*, 1996, 2014]. Most of the ∼60 samples were collected into 34 L internally electropolished stainless steel canisters using cryogenic techniques. The CGAA samples were analyzed in 2006 on a laboratory-based Medusa-GCMS at CSIRO (Medusa-9), and all samples collected since 2004 have since been analyzed on the Cape Grim based Medusa-3.

We also include Medusa-GCMS measurements from archived air samples of the Northern Hemisphere, which were collected at several stations in the U.S. and analyzed at SIO on Medusa-1. The samples were mostly collected during clean air conditions but for purposes other than creating a consistent archive for trace gas histories. For this reason, the data set needed more careful processing [e.g., *Mühle et al.*, 2010; *Rigby et al.*, 2010]. A stepwise tightening filtering algorithm was applied for the measurement results based on their deviations from a fit through all data (including in situ data), which resulted in the rejection of 1–10% of the data (depending on the compound). Due to the scarcity of the Northern Hemisphere halon data, the filtering of these samples used the fit through the filtered Southern Hemisphere samples as additional guide (with an appropriate time lag related to hemispheric transport). The final data set showed good agreement with concurrent in situ measurements, when available. Numerical results from the analysis of the archived air samples are given in the supporting information.

2.4. Air Entrapped in Firn

Firn is the porous layer of unconsolidated snow overlaying an ice sheet. Air is present in tiny channels that for most of the firn are in contact with the atmosphere. Air in the channels mixes very slowly by diffusion, down

Table 3. The Time Evolution of Instrumentation Used for the Analysis of Halons in Flasks at the National Oceanic and Atmospheric Administration/Global Monitoring Division (NOAA/GMD)

Halon	Time Period	Instrument	Method Information
H-1211	1988–2006	GC-ECD	*Butler et al.* [1998]
	1992 to present	GCMS-1 and 3[a]	0.2 L, −145°C to −165°C, 60 m DB-5
H-1301	1988–2006	GC-ECD[b]	*Butler et al.* [1998]
	2004–2007	GCMS-1[a]	0.8 L, −145°C to −165°C, 60 m DB-5
			Ascarite in line to remove carbon dioxide
	2007 to present	GCMS-2[c]	0.2 L, −145°C to −165°C, 30 m GasPro
H-2402	1995–1997	GCMS-1[a]	Same as H-1211 during this period
	2004–2007	GCMS-1[a]	Same as H-1301 during this period
	2009 to present	GCMS-3[a]	Same H-1211 during this period

[a]GCMS-1 (M1) was a Hewlett-Packard 5971A MS. GCMS-3 (M3) is an updated version of GCMS-1: In 2009 the MS on GCMS-1 was upgraded to an Agilent 5973; a new DB-5 column was installed concurrently.
[b]Also known as the LEAPS/ECD; these results from *Butler et al.* [1998] as updated online at ftp://ftp.cmdl.noaa.gov/hats/halons/flasks/stations_ECD/ have been adjusted by the multiplicative factor 1.028 based on comparisons with the GCMS results to provide a consistent record over time.
[c]GCMS-2 is also referred to as M2.

to near the bottom of the firn layer where diffusion ceases and the air is locked in. The air can be extracted and measured to reconstruct past atmospheric composition [e.g., *Schwander et al.*, 1993]. H-1211 and H-1301 measurements in firn air were first made by *Butler et al.* [1999] and demonstrated the purely anthropogenic nature of their emissions.

For the first time in our combined AGAGE/NOAA analysis we also include measurements of air entrapped in polar firn from both hemispheres (Table 2 and Figure 1). From Antarctica we include samples from six depths collected in 1997–1998 at the DSSW20K site (66.77°S, 112.35°, 1200 mean annual sea level (MASL), and ∼20 km west of the deep Dome Summit South drill site near the summit of Law Dome, East Antarctica [*Trudinger et al.*, 2002; *Sturrock et al.*, 2002]) and one deep sample from the South Pole [*Butler et al.*, 2001]. The Northern Hemisphere firn air samples considered here were collected near the northwest Greenland ice drill site NEEM (North Greenland Eemian Ice Drilling) at 77.45°N, 51.06°W, and 2484 MASL in 2008 (NEEM-2008, EU hole) [*Buizert et al.*, 2012]. Samples were pumped without drying into electropolished stainless steel canisters. Results for H-1211 and H-1301 from DSSW20K have been previously reported, based on the analysis of similar or equal subsamples on different instruments (ADS-GCMS) [*Sturrock et al.*, 2002]. All other firn air results are the first reported for these samples. Measurements of halons have been made at NOAA from numerous other firn sampling expeditions but are not discussed further here (see supporting information).

The firn air samples were analyzed in March 2012 at CSIRO on Medusa-9. All firn air samples available at CSIRO at that time were analyzed for a suite of ∼50 halogenated trace gases. Measured sample volumes and replicate analysis depended on the availability of the sample quantities and varied between 1 L and 3 L and 2–3 replicate analyses of each sample. All samples were alternatingly measured versus a single tertiary calibration tank (T-EMPA-1) linked into the AGAGE calibration system. The analytical system used for this analysis deviated from the in situ Medusa-GCMSs mainly by the use of different chromatographic columns for compound separation. For this analysis we used GS-GasPro capillary columns with a main column (0.32 mm ID × 60 m, Agilent Technologies) as described by *Ivy et al.* [2012]. However, an additional GS-Gaspro precolumn (0.32 mm ID × 5 m) was installed, which allowed for a backflushing of late eluting compounds. Numerical results for the firn air measurements are given in the supporting information.

2.5. NOAA Sampling, Measurement Techniques, and Instrument Calibrations

Halons have been measured by NOAA using several different sampling and measurement techniques over time (Table 3 and Figure 1). Results used in this analysis are based on collection of samples in flasks with subsequent analysis using GCMS or, in earlier years, GC electron capture detector (GC-ECD) instrumentation. Measurements of H-1211 have also been obtained with in situ instrumentation using GC-ECD techniques (termed "Chromatograph for Atmospheric Trace Species (CATS) ECD").

For the halon measurements reported here, flask samples have been collected in pairs from 12 stations around the globe with the longest record dating back to the late 1980s for GC-ECD analysis of flasks and early 1992 for GCMS analyses of flasks (see *Butler et al.* [1998] and Table 2). Samples are routinely collected at the stations in pairs (without drying) in 0.85 L to 3 L internally electropolished stainless steel flasks compressed to 2.5 bar using a membrane pump (KNF Neuberger Model UN05SV1). Glass flasks are also collected at a subset of sites and are typically pressurized to 1.5–2 bar. The flasks are analyzed in the NOAA/ESRL/GMD Boulder Laboratories. The sample aliquots (typically 0.2 L) are cryocondensed using an uncoated 0.53 mm I.D. fused silica tubing maintained at −145°C to −165°C. The cryofocused samples are subsequently desorbed onto a 60 m DB-5 capillary column. More details are given in *Montzka et al.* [1993], *Butler et al.* [1998], and Table 3. The MS was upgraded to an Agilent 5973 quadrupole MS and a new 60 m DB-5 capillary column in mid-2009. The analysis of H-1301 from the flask samples has been conducted on multiple GCMS instruments since 2004 using similar technology as described in *Montzka et al.* [1993].

Working standards (std) are used as a direct reference for flask measurements in the injection sequence: std, flask 1, flask 1, std, flask 2, flask 2, std, etc., where "flask 1" and "flask 2" represent two aliquots analyzed from each individual flask of each sampled pair. The working standards are cylinders pressurized to 100–136 bar with oil-less compressors (Rix Industries) at Niwot Ridge, Colorado, and, in the case of H-1211 and H-1301, have been calibrated by multiple comparisons to a suite of gravimetric standards with the assumption of linear response (see section 2.6 for more details). During the ongoing measurement period (since 1992), a total of 13 secondary high-pressure reference cylinders have been used sequentially to provide a reference for the flask analysis.

The NOAA data presented here represent extensions of records initially published by *Butler et al.* [1992, 1998]. They have been updated in subsequent papers [e.g., *Montzka et al.*, 2003] and have been used in the determination of equivalent effective stratospheric chlorine (EESC) trends over time [*Hofmann and Montzka*, 2009] which is regularly updated at http://www.esrl.noaa.gov/gmd/odgi/. NOAA data through 2012 appeared in *Carpenter and Reimann* [2014].

For in situ analysis of H-1211, the sampling uncertainty is estimated as 0.5% based on measurement repeatability of the on-site calibration standards (tertiary level). For flask analyses by GCMS, pair means are reported with an uncertainty derived from the apparent difference measured between the individual flasks. Median relative measurement precisions (1σ) as determined from replicate flask analysis have been 0.36% for H-1211 (on GCMS-3 since 2009), 1.0% for H-1301 (on GCMS-2 since 2007), and 1.6% for H-2402 (on GCMS-3 since 2009; see Table 3).

2.6. Halon Calibration Scales

The AGAGE measurements for H-1211 and H-1301 are reported on the SIO-05 primary calibration scales. These scales are defined through the gravimetric preparation of 13 synthetic primary standards at near-ambient mole fractions [*Prinn et al.*, 2000] at SIO in 2005. By comparing their relative assigned mole fractions and measurement results, an internal agreement of ∼0.5% is estimated for each of the two halons. The accuracies of these primary standards sets are estimated at 3% (1σ), for H-1211 and H-1301, with the largest fractional uncertainty contributed from the impurity of the starting reagent. In 2014, SIO generated the SIO-14 primary calibration scale for H-2402 based on the gravimetric preparation of three synthetic primary standards near 1.2 ppt (parts per trillion, 10^{-12}, in dry air) with an internal agreement of 0.98%. The accuracy of this primary standards set is also estimated at 3%. This new H-2402 calibration scale allows for the first independent reporting of AGAGE H-2402 data, which previously had been disseminated based on the NOAA calibration scale. These H-2402 data are now released into public data repositories on the SIO-14 calibration scale.

NOAA has recently updated their H-1211 and H-1301 scales developed in the 1990s to NOAA-2006, which is based on the preparation of new synthetic primary standards. For H-1211 NOAA-2006 is defined through a set of four primary standards at near-ambient mole fractions, showing an internal consistency in response per parts per trillion of <1% (1σ). The accuracy of the H-1211 NOAA-2006 calibration scale is estimated at 1.5% (1σ). A conversion factor of 1.011 has been determined for H-1211 to convert the data from the older NOAA-1996 scale to the NOAA-2006 scale (Table 4). For H-1301, NOAA-2006 is defined through a set of seven primary standards at near-ambient mole fractions. For the ECD measurements of those five standards with mole fractions below 5 ppt, an internal agreement of ∼3% is estimated with respect to their assigned mole fractions. For the GCMS measurements and using all seven primary standards, the internal agreement is

Table 4. Primary Scale Conversion Factors for the Halons H-1211 ($CBrClF_2$), H-1301 ($CBrF_3$), and H-2402 ($CBrF_2CBrF_2$)[a]

	H-1211 SIO-05	H-1301 SIO-05	H-2402 SIO-14	H-1211 NOAA-2006	H-1301 NOAA-2006	H-2402 NOAA-1992
H-1211 NOAA-2006	1.020[b,c]	–	–	–	–	–
H-1301 NOAA-2006	–	1.025[c]	–	–	–	–
H-2402 NOAA-1992	–	–	0.981[d]	–	–	–
H-1211 NOAA-1996	1.031[d]	–	–	1.011[e]	–	–
H-1301 NOAA-1990	–	1.158[d]	–	–	1.13[e]	–
H-1211 UEA	0.908[f]	–	–	0.89[g]	–	–
H-1301 UEA	–	1.22[h]	–	–	1.19[g]	–
H-2402 UEA	–	–	1.14[i]	–	–	1.15[i]
H-1211 UM/NCAR	1.047[k]	–	–	1.026[j]	–	–
H-1301 UM/NCAR	–	1.077[k]	–	–	1.050[j]	–
H-2402 UM/NCAR	–	–	1.060[k]	–	–	1.081[j]

[a]Example for using conversion factors: To convert from H-1211 measurement results reported on NOAA-2006 to results reported on SIO-05, multiply them by 1.020. SIO: Scripps Institution of Oceanography, NOAA: National Oceanic and Atmospheric Administration, UEA: The University of East Anglia, UM/NCAR: The University of Miami/National Center for Atmospheric Research.
[b]Applies to the NOAA GCMS flask data (see Table 2). For the NOAA CATS ECD data, the conversion factor is 1.008.
[c]Derived from in situ intercomparisons of the two networks and from the International Halocarbons in Air Comparison Experiment (IHALACE), see *Hall et al.* [2014].
[d]This work, see text.
[e]B. Hall, personal communication, 2015.
[f]Derived from the UEA to NOAA-2006 conversion [*Newland et al.*, 2013] and the NOAA-2006 to SIO-05 conversion (this work). This agrees reasonably well with the UEA to SIO-05 conversion factor of 0.893 reported by *Reeves et al.* [2005].
[g]From *Newland et al.* [2013]. These factors for H-1211 and H-1301 were by mistake interchanged in the text of *Newland et al.* [2013] (M. Newland, personal communication, 2015)
[h]Derived from the UEA to NOAA-2006 conversion [*Newland et al.*, 2013] and the NOAA-2006 to SIO-05 conversion (this work). This agrees reasonably well with the UEA to SIO-05 conversion factor of 1.27 reported by *Reeves et al.* [2005].
[i]Based on our comparison of Cape Grim Air Archive (CGAA) measurements reported by *Newland et al.* [2013] on the UEA scale and those reported in this study (SIO-14). These factors only apply to the results published by *Newland et al.* [2013]. For the results published by *Fraser et al.* [1999], we derive a conversion SIO-14-reported = 0.035 ppt + 1.053 × UEA-reported.
[j]From IHALACE [*Hall et al.*, 2014].
[k]Calculated from (j) and the present NOAA to SIO conversions.

~1.4%. The accuracy of the H-1301 NOAA-2006 calibration scale is estimated at ~2% (1σ) with the main fraction of the uncertainty related to reagent purity. A conversion factor of 1.13 has been determined for H-1301 to convert data from the older (NOAA-1990) scale to NOAA-2006.

For H-2402, the NOAA-1992 calibration scale is defined through a single synthetic primary standard prepared with gravimetric techniques in 1992 at a mole fraction substantially above ambient air values (47.5 ppt). Calibrations initially applied to whole-air reference standards were subsequently propagated to a suite of whole-air standards, thereby replacing the original primary standard in its function. These whole-air standards are now defining this calibration scale. The accuracy for the H-2402 calibration scale is estimated at 15%, with the largest fractional uncertainties from the weighing of the reference material and poorly understood purity of the raw material.

To bring the AGAGE and NOAA data together so that they provide a consistent and comprehensive view of halon atmospheric distributions and changes over time, we determine calibration scale differences in the form of scale factors that are applied to the results from one network (Table 4). The comparisons are based on field observations from the colocated measurement sites Mace Head, Trinidad Head, Cape Matatula, and Cape Grim (AGAGE ADS/Medusa-GCMS and NOAA flask results) for 1998–2015 for H-1211 and 2004–2015 for H-1301 and H-2402. Based on these intercomparisons and also using the results from the laboratory intercomparison of the International Halocarbon in Air Comparison Experiment [*Hall et al.*, 2014], the average conversion factor from NOAA-2006 to SIO-05 for H-1211 is 1.016 ± 0.007 (for the NOAA GCMS flask data only, this factor is

1.020 and for the CATS ECD data only, the factor is 1.008). For H-1301, the NOAA-to-SIO conversion factor is 1.025 ± 0.011 (Table 4) for both NOAA data sets. For H-2402 the conversion factor is 0.981 ± 0.010 based on colocated measurements at four sites between 2009 and 2015.

For completeness, we also list the conversion factors for the University of East Anglia's (UEA) calibration scales [*Newland et al.*, 2013] and for the University of Irvine calibration scales (Table 4) [*Hall et al.*, 2014]. If we convert the recent [*Newland et al.*, 2013] CGAA UEA measurement results for H-1211 and H-1301 (reported on NOAA-2006 calibration scales) to the SIO-05 scales, we then find good agreement with our own measurements of the CGAA samples. A basic comparison of the two CGAA data sets for H-2402 suggests a SIO-14/UEA scale conversion factor of 1.14 and a NOAA-1992/UEA scale conversion factor of 1.15 (Table 4). As already noted by *Newland et al.* [2013], the older CGAA H-2402 UEA measurement results reported earlier by *Fraser et al.* [1999] on the UEA scale cannot be converted to the NOAA-1992 (or SIO-14) scales with constant conversion factors presumably due to a nonlinearity effect. To convert these older H-2402 measurements to the SIO-14 calibration scale, we derive a relationship SIO-14 reported = 0.035 ppt + 1.053 × UEA reported.

2.7. Uncertainties of the Reported Measurements

We derive the accuracies for the reported measurements from three independent uncertainties. These include the previously mentioned calibration uncertainties and the uncertainties related to the on-site measurements (repeatabilities). In addition, uncertainties related to the scale propagation through transfer standards need to be taken into account, in particular for the AGAGE network where the hierarchical propagation from the primary to the quaternary standards can add larger uncertainties than are found for the on-site reproducibilities. For comparisons on measurements conducted on the same calibration scale, the overall uncertainties are much smaller because then the uncertainty of the calibration scale should be ignored. A more detailed analysis is discussed in the supporting information.

For the AGAGE network data, the propagation uncertainties are estimated to be 1% for H-1211 and 3% declining to 2% with new MSs for both H-1301 and H-2402. The overall accuracies based on the three types of individual uncertainties then amount to 3.5% for H-1211, 4.5% for H-1301, and 5% for H-2402.

For the NOAA network the scale propagation uncertainties are estimated to be 0.1% for H-1211 and 0.2% for both H-1301 and H-2402. When combined with the scaled uncertainties and the measurement precisions, overall accuracies of the reported data are 1.8% for H-1211, 2.6% for H-1301, and 15% for H-2402.

2.8. Bottom-Up Inventory-Based Emission Estimates

Bottom-up emission estimates are based on industry and governmental data on the production, distribution, and usage of these compounds. We discuss these independent emission estimates because they are helpful as a priori data sets in our model analysis and to compare them with our observation-based top-down estimates. Because of their usage in fire-fighting equipment, the derivation of emissions from production and consumption data is difficult given the large and long-lasting banks of these compounds [*HTOC*, 2011; *Verdonik and Robin*, 2004]. Also, in recent years, trading of recycled halons appears to have become an important part of the halon budgeting [*HTOC*, 2011], which adds to the difficulties of estimating emissions from usage data. It is likely that the emission functions have changed significantly through time due to changing handling practices of the equipment. The details of the derivation of production and emission estimates are often not published in full and lack sufficient transparency.

Historic bottom-up production and emission estimates for H-1211 and H-1301 are available from *Fraser et al.* [1999], which are partially based on the analysis by *McCulloch* [1992]. Independent estimates were also published by the HTOC with several updates [e.g., *HTOC*, 2007, 2011] with the latest updates in 2014 [*HTOC*, 2014a; unpublished numerical data provided by D. Verdonik, 2015]. In the past, bottom-up inventory-based H-2402 emission data were sparse [*HTOC*, 2011] and appeared to be erroneously low with emissions estimates at least a factor 10 lower compared to top-down (observation-based) emissions estimates [*Montzka et al.*, 2011]. However, the HTOC has recently significantly revised its production and emission estimates for H-2402 based on updated information for Russia, which was the major producer of this compound [*HTOC*, 2014a; *Kopylov et al.*, 2003].

For the present study we use the HTOC 2014 emission data for all three halons [*HTOC*, 2014a] (numerical data unpublished) as a priori input for the model calculations. These HTOC 2014 and earlier data published by HTOC [*HTOC*, 2011], which we also compare our results with, were verified to have been derived independently from any previous atmospheric observation-based emission estimates [e.g., *Carpenter and Reimann*, 2014].
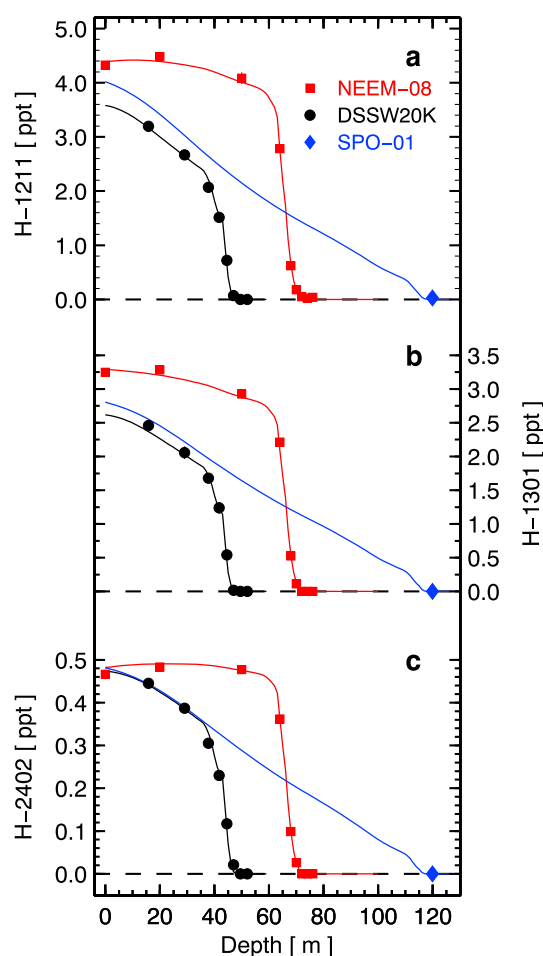
Figure 2. Depth profiles for the three halons (a) H-1211, (b) H-1301, and (c) H-2402 in polar firn. Measured dry air mole fractions are shown for the Greenland site NEEM-08 (red squares) and the Antarctic sites Law Dome (DSSW20K, black circles) and South Pole (SPO-01, blue diamond). Generally, the measurement precisions (1σ) are smaller than the plotting symbols. The measurements are plotted on the respective SIO calibration scales. The modeled mole fraction depth profiles (solid lines) correspond to the optimized emissions history from the CSIRO inversion, derived from the combined observations of all three firn sites, archived air, and in situ measurements.

2.9. Firn Model, Global Chemical Transport Models, and Inverse Method (Top-Down Emission Estimates)

In this study we use different model approaches for various parts of our investigation. First, the dating of firn air measurements requires a model of the physical processes occurring in the firn. Second, a global model of atmospheric transport and chemistry was used to simulate mole fractions due to surface emissions. Third, the atmospheric and firn models were both used in global inversion calculations to give observation-based top-down emissions estimates with uncertainties. Finally, we use a Lagrangian transport model to track H-2402 pollution events measured at the Gosan station. The models and inversion approaches are briefly explained next.

2.9.1. Firn Model

Unlike air collected directly from the atmosphere, firn air samples do not have a discrete age but rather an age distribution that depends on the physical processes that occur in the firn. We use the CSIRO firn model [*Trudinger et al.*, 1997, 2013] to quantify these processes. The most important process occurring in firn is molecular diffusion of air through the open pores in the firn column. The diffusion decreases with depth and eventually stops in the "lock-in zone."

As it is linear, the firn model can be represented by Green's functions (also called age distributions or age spectra) that relate the mole fraction at any depth in the firn to the mole fraction in the overlying atmosphere over a range of years [*Rommelaere et al.*, 1997; *Trudinger et al.*, 2002]. Green's functions from the firn model are

used in the inversion calculations to relate the firn measurements to high-latitude mole fraction. Uncertainty in the firn model can be incorporated into inversion calculations by the use of ensembles of Green's functions that represent the uncertainty in model parameters and physical processes [*Trudinger et al.*, 2013].

Although the age of firn air is best characterized by a distribution, it can be useful sometimes to assign a single age to a firn sample, particularly for graphical purposes. Two quantities that are useful here are the mean age (the mean of an age distribution) and the effective age (this takes into account variations in atmospheric growth rate and is the most useful estimate of the age of a firn measurement) [*Trudinger et al.*, 2002]. Note that the full age distributions should be used in inversion calculations, which is also done in the present analysis.

The measurement results for the firn air samples at all three sites are shown in Figure 2 where they are plotted against depth. They are compared to the modeled mole fraction depth profiles calculated with the optimized emissions history from the CSIRO inversion. Note that an individual depth profile is not based on the observations of that site alone but based on observations from all three firn sites, the archived air, and in situ measurements together.

2.9.2. AGAGE-12 Box Atmospheric Model

The AGAGE 12-box two-dimensional model of atmospheric transport and chemistry [*Cunnold et al.*, 1983, 1997; *Rigby et al.*, 2013] was used to estimate the concentration of each gas in three vertical layers of the atmosphere (separated at 500hPa and 200hPa) and four semihemispheric boxes separated at the equator and at 30°. These latitudinal separations result in equal air masses in each of the semihemispheric boxes of the respective layers. The model transport parameters, OH concentration, and photolytic loss were assumed to be seasonally varying and interannually repeating [*Spivakovsky et al.*, 2000; *Rigby et al.*, 2013]. Loss in the atmosphere is dominated by the photolytic sink for these compounds, which was assumed to follow the same seasonal cycle as the OH loss in the troposphere but with a magnitude that was tuned to reflect the current best estimate lifetimes of these compounds from *SPARC* [2013]. The loss in the stratosphere was assumed to be constant, although the stratosphere-troposphere exchange rate varies with time. For the lifetimes we use the best estimate lifetimes from *SPARC* [2013] shown in Table 1. For the uncertainties we use half of the "possible ranges" derived by *SPARC* [2013], which were derived as the span of 2σ uncertainties from several methods applied in that study.

2.9.3. Global Inversion Methods

To estimate global emissions through time, two different Bayesian inverse methods ("Bristol" and "CSIRO") were used both using the AGAGE 12-box atmospheric transport model to relate surface emissions and atmospheric mole fraction. The Bristol inversion, which has been used for many similar studies [e.g., *Rigby et al.*, 2011; *Vollmer et al.*, 2011; *Rigby et al.*, 2014; *O'Doherty et al.*, 2014; *Vollmer et al.*, 2015], is targeted predominately at the in situ measurements on a monthly timescale and semihemispheric spatial scale but here for the first time is extended to include the firn air measurements. The CSIRO inversion is targeted at the annual timescale and global spatial scale and was developed predominantly for analysis of firn and ice core air measurements to estimate global emissions and mole fraction prior to direct atmospheric measurements [*Trudinger et al.*, 2002; C. M. Trudinger et al., manuscript in preparation, 2016].

Both inversions estimate emissions using the measurements and model-calculated sensitivities of changes in atmospheric and firn mole fractions to changes in emissions. For the firn air samples, we first estimated the sensitivity of changes of the mole fraction that would be observed in the firn to changes in atmospheric concentrations and then calculated the sensitivity of these atmospheric concentrations to changes in emissions. The overall sensitivity of the firn observations to changes in surface flux was then the product of these two factors (C. M. Trudinger et al., manuscript in preparation, 2016). As a priori information, both inversions use the bottom-up inventory-based HTOC 2014 [*HTOC*, 2014a] (numeric data unpublished) emission estimates for all three halons.

The Bristol inversion uses information from the firn, archived, and in situ air samples in a single inversion in which the rate of growth of emissions was constrained by an a priori estimate and then adjusted based on the observations [*Rigby et al.*, 2011, 2014]. Of the in situ measurements, only Mace Head, Trinidad Head, Ragged Point, American Samoa, and Cape Grim were used for the inversion. Uncertainties in the Bristol inversions were calculated following the method in *Rigby et al.* [2014], in which the derived emission uncertainties include contributions from the observations, the atmospheric and firn models, the calibration scale, and the assumed lifetimes. Following *Rigby et al.* [2014], model representation errors in the Bristol inversion were assumed to be equal to the monthly mean variability in the high-frequency baseline observations. Where high-frequency

observations were not available (e.g., for the firn or archive data), this term was assumed to be equal to the mean baseline variability from the in situ data in that semihemisphere scaled by the measured mole fraction.

The CSIRO inversion uses the firn observations and annual values sampled from a spline fit to the in situ (Mace Head and Cape Grim only) and archive measurements in a Bayesian synthesis inversion to infer annual global emissions. A particular challenge for inverting firn and ice core measurements is that emissions and mole fractions at annual resolution are not well constrained, as unrealistic oscillations in mole fraction would not be inconsistent with the firn measurements [*Rommelaere et al.*, 1997] but would be inconsistent with our understanding of the atmospheric budget and how quickly global atmospheric mole fractions can change with time. Inversion of firn measurements needs some kind of regularization to keep annual variability to a realistic level. In the CSIRO inversion we use a constrained inversion that excludes negative emissions and mole fractions, and we also include a penalty in the inversion for solutions with unrealistically large year-to-year variability. These "reality" constraints narrow the uncertainty range, which would otherwise be overestimated. We estimate the uncertainty in emissions inferred with the CSIRO inversion using a bootstrapping method and also by incorporating firn model uncertainty through the use of an ensemble of firn Green's functions.

2.9.4. FLEXPART Analysis for Source Allocation of H-2402 Pollution Events

H-2402 pollution events were only detected at Gosan and to a lesser degree at Shangdianzi. In order to locate potential sources in the northeastern Asian region, we applied the Lagrangian Particle Dispersion Model (LPDM) FLEXPART [*Stohl et al.*, 2005] in backward mode. For each 3-hourly time interval and measurement site, 50,000 particles were released for the periods between January 2010 and December 2014 (Gosan) and May 2010 and August 2012 (Shangdianzi). FLEXPART was driven by global wind fields obtained from the European Centre for Medium-Range Weather Forecasts (ECMWF) operational analysis and forecasting system. For each individual backward run, the source-receptor relationship (SRR) at the surface (also termed footprints or source sensitivities) was obtained by evaluating the model particles' residence time along the backward trajectories [*Seibert and Frank*, 2004].

We then combined the H-2402 observations with the footprints by computing the average footprints, H, corresponding to all H-2402 observations from both sites that were larger than the baseline by 0.02 ppt. The baseline was determined separately for each of the two sites by applying the robust extraction of baseline signal (REBS) filter algorithm described by *Ruckstuhl et al.* [2012] (Note that this is a different filter than that applied for the publicly archived AGAGE monthly mean halon data.) In addition, the average footprint of all observations, T, was calculated. The normalized difference between this average "polluted" footprint and the average footprint of all observations, $(H - T)/T$, was used to detect areas with potential H-2402 emissions. This approach is equivalent to classical back trajectory analysis to detect potential source areas [e.g., *Ashbaugh et al.*, 1985] but much more robust due to the use of the more sophisticated LPDM simulations. A positive value of the normalized difference indicates areas to which the observations were more sensitive during pollution events than on average. In reverse this qualitatively indicates a potential source in these areas.

3. Results and Discussion

3.1. Atmospheric Histories

By combining our archived air (including firn) and recent in situ measurements we produce atmospheric histories of nearly nine decades for the three halons. These results are shown in Figures 3–5. The firn air samples in Figure 3 are plotted against effective ages (unless mole fraction is zero or near zero, when mean ages are used) [see *Trudinger et al.*, 2002]. The AGAGE ADS-GCMS and Medusa-GCMS results (Figure 4) are monthly means of background-filtered data (results deemed representative of broad atmospheric regions) following a statistical filter algorithm [*O'Doherty et al.*, 2001; *Cunnold et al.*, 2002]. Some of these results from the stations with frequent regional pollution events are biased toward higher monthly means (e.g., Monte Cimone and Shangdianzi) due to some limitations in the filter algorithm. Also, ADS-GCMS measurements were less precise than those by Medusa-GCMS, resulting in larger standard deviations in the earlier part of the in situ record, particularly for H-1301. H-2402 ADS-GCMS results, shown in Figure 4 for Cape Grim only, are not used for the inversion but shown here to demonstrate the improvement in the measurement technology. Results from the NOAA network are shown in Figure 5 for a few selected stations including those at high latitudes where no AGAGE measurements are available. The NOAA results also show significant improvements in measurement consistency over time as new instruments came into use (see Table 3). When converting the NOAA measurements to the SIO calibration scales on which the AGAGE measurements are reported, we find agreement within the combined uncertainties between the data sets for the colocated sites and overlapping periods.
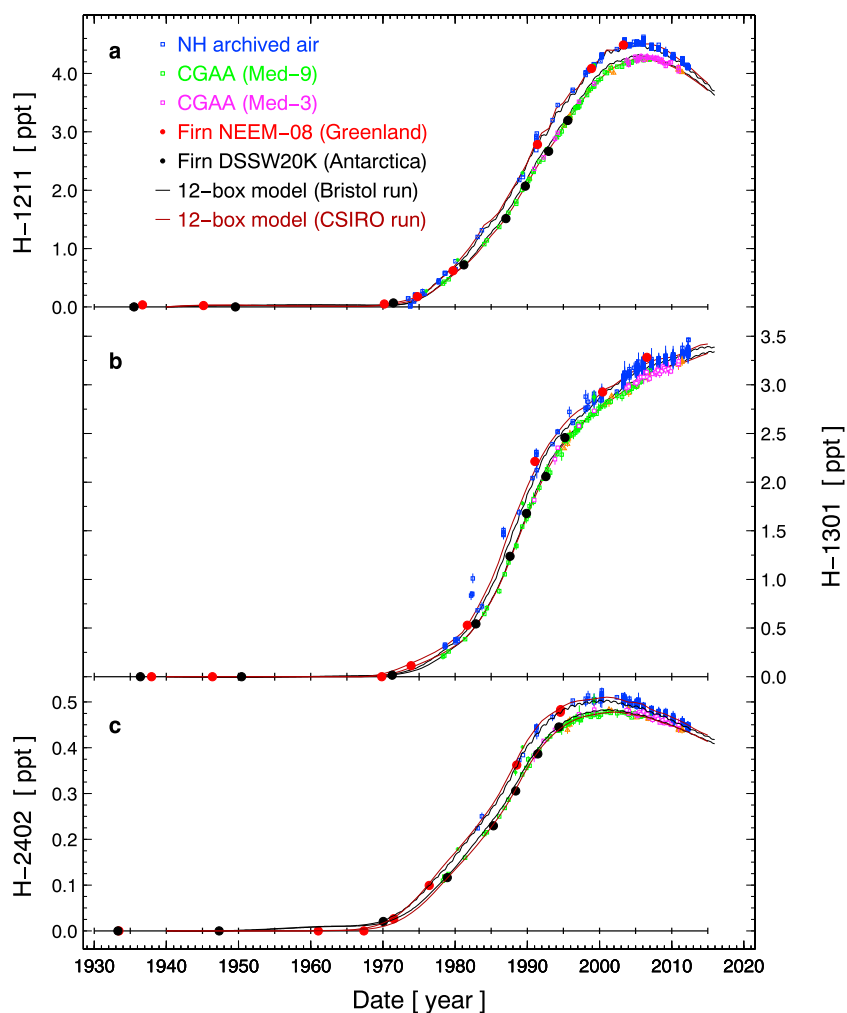
Figure 3. Atmospheric histories of the halons (a) H-1211, (b) H-1301, and (c) H-2402 from archived air samples and firn. Open squares show the archived air samples from the Northern Hemisphere (blue) and from the Southern Hemisphere (Cape Grim Air Archive, CGAA, in green and magenta). Their vertical bars denote the measurement precisions (1σ), which are often smaller than the plotting symbol. Filled circles show measurements of air entrapped in polar firn from Greenland (NEEM-08, red) and Antarctica (DSSW20K, black). The solid lines denote the modeled mole fractions for the two hemispheres based on the 12-box AGAGE model (independently run by Bristol and CSIRO) and are based on the data shown here and on the AGAGE in situ measurements and the King Sejong Antarctica flask samples. The measurements are plotted on the SIO primary calibration scales for the halons.

Also, the results from the Antarctic King Sejong station (Figure 1 and Table 2) agree with the Cape Grim results within the precisions of the measurements suggesting an absence of sources and a well-mixed troposphere in the midlatitude to high-latitude Southern Hemisphere.

These histories show the atmospheric onsets of all three halons in the late 1960s to early 1970s followed by rapid increases over the subsequent decades (Figure 3) with maximum growth rates in the late 1980s. Owing to both voluntary and regulatory actions to reduce unnecessary and emissive uses of these halons, their growth rates have slowed down and the atmospheric mole fractions of H-1211 and H-2402 started to decline within the past one to two decades. For the period 1930s to 1960s, all three halons are undetectable (<0.03 ppt) in the remote atmosphere as shown from the deepest polar firn air samples suggesting that the compounds are entirely of anthropogenic origin. This conclusion is consistent with previous findings [*Butler et al.*, 1999; *Sturrock et al.*, 2002; *Reeves et al.*, 2005].

3.1.1. H-1211

H-1211 reached maximum mole fractions in the Northern Hemisphere in the mid-2000s at about 4.5 ppt (Figures 4 and 5). Since then, the mole fractions have declined to a global mean of 3.8 ppt by 2015.
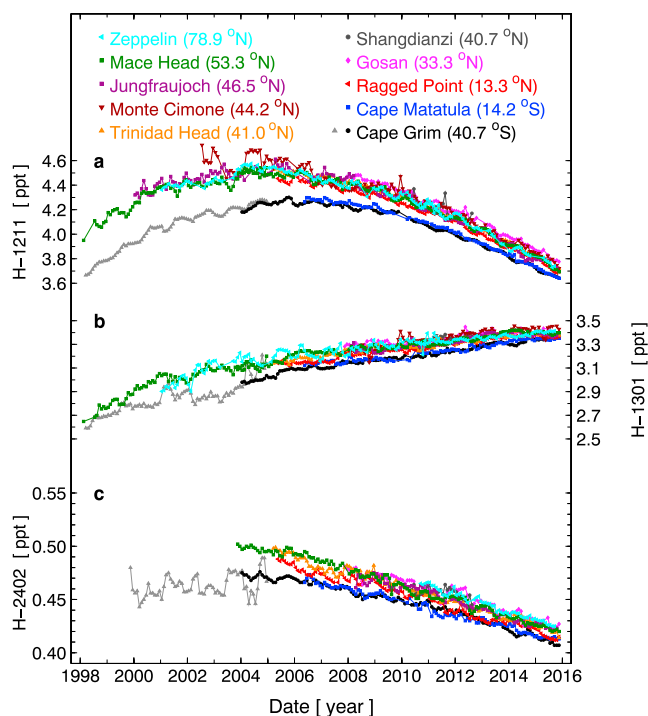
Figure 4. Monthly means of the atmospheric records of the AGAGE results from the in situ measurements at 10 stations for the halons (a) H-1211, (b) H-1301, and (c) H-2402. These monthly means are based on background data (deemed representative of broad atmospheric regions) only. Some of the early records are based on ADS-GCMS measurements with overlap to Medusa-GCMS (see Table 2). The early Cape Grim H-2402 data (in gray, upward triangles, 1999–2004) are shown here only to demonstrate instrumental improvement from ADS (adsorption-desorption system) to Medusa-GCMS instruments but are not used in the model calculations. Standard deviations of monthly means are not shown here for clarity reasons. The measurements are plotted on the SIO primary calibration scales for the halons.

The interhemispheric gradient, caused by the predominantly Northern Hemisphere emissions, has reduced to ~0.2 ppt by 2015 mainly because of the decreased global emissions and partly due to the equatorward shift of Northern Hemisphere emissions [*Reeves et al.*, 2005]. There is also some seasonality in the records, which is believed to be caused predominantly by the seasonalities of the photolytic sink in the troposphere and the atmospheric mixing processes.

The AGAGE 2-hourly air measurements allow us to detect regional pollution events and to track their frequencies, magnitudes, and durations over the years of measurements. For some of the stations discussed in this paper, we still find pronounced pollution events in the more recent parts of the records indicating ongoing emissions. For H-1211, pollution events are detected at Mace Head during advection of continental European air, and at Jungfraujoch, with typical magnitudes of 0.5–1 ppt above the background levels. There is no obvious trend of declining frequencies or magnitudes of these events over the last decade suggesting that H-1211 is still banked and released in significant quantities in Europe. At Shangdianzi, where our record is limited to May 2010 to August 2012, frequent pollution events were detected (typically 2 ppt above background) during southerly advection, which includes air masses from the Beijing area. Pollution events from China and to some extent from the Korean peninsula are also detected at Gosan. By comparison, pollution events at Trinidad Head and Cape Grim are much less frequent and lower in magnitude, and they are virtually absent at Ny Ålesund, Ragged Point, and Cape Matatula.

3.1.2. H-1301
H-1301 mole fractions are still growing in the atmosphere and have reached a global mean of 3.4 ppt in 2015. Due to its long lifetime (72 years), small emissions are sufficient to maintain this growth. However, the growth rate has decreased from 0.20 ppt yr^{-1} in the late 1980s to less than 0.015 ppt yr^{-1} in 2013–2015. The high-frequency data of the AGAGE stations show a different picture compared to H-1211. For H-1301, pollution events at Mace Head are much less frequent and have declined in magnitude over time, and they are virtually absent at Jungfraujoch. Shangdianzi and Gosan show similar pollution sectors as for H-1211
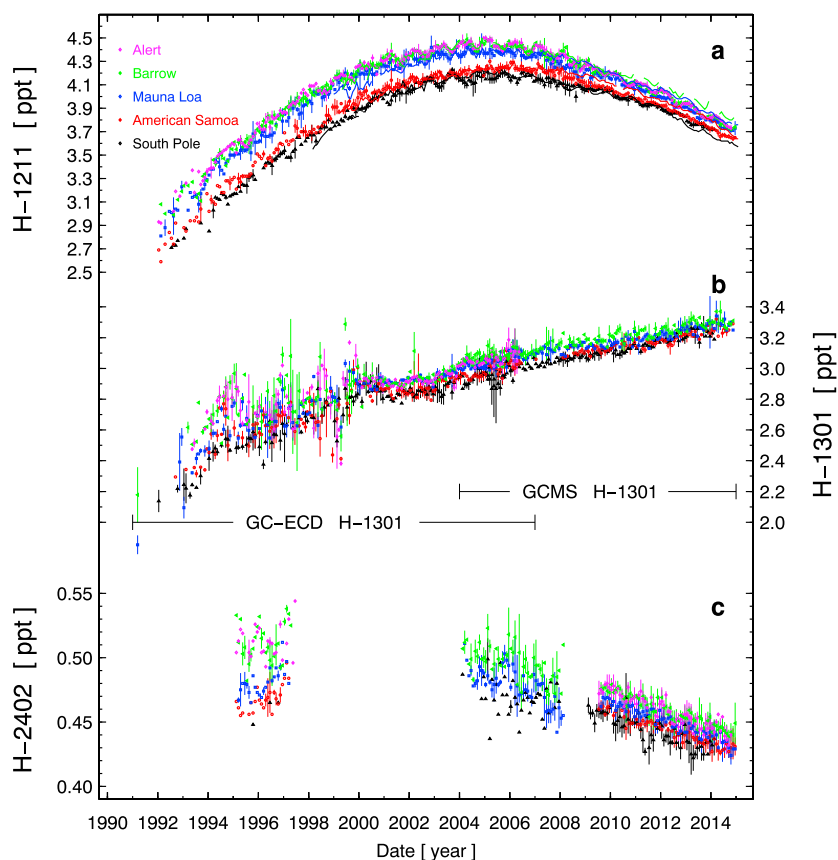
Figure 5. NOAA-measured monthly mean dry air mole fractions and standard deviations for the halons (a) H-1211, (b) H-1301, and (c) H-2402. For clarity, results displayed here represent only a subset of sites where flask measurements of halons and other compounds are regularly made. For H-1211, results from the CATS GC-ECD in situ instruments are also included as lines without uncertainties. The flask measurements for each of these compounds represent results from different instruments at different times in the past; see section 2.5 and Table 3 for more details. Flask sampling at these sites is limited to periods when air is from a clean air sector. Results deemed nonrepresentative of broad atmospheric regions are not included in the monthly means. The measurements are plotted on the NOAA primary calibration scales for the halons. Note that the GC-ECD data for H-1301 have been multiplied by the factor 1.028 to provide a consistent record over time (see section 2.5).

but also with significantly smaller frequencies compared to H-1211. Ny Ålesund, Ragged Point, and Cape Matatula all show no H-1301 pollution events during Medusa-GCMS measurements, and at Trinidad Head, pollution events exceeding 1 ppt from the baseline were limited to five events for the entire Medusa-GCMS record. At Cape Grim there are indications of small H-1301 pollution events in air masses that had previously passed over the Melbourne/Port Phillip area.

3.1.3. H-2402

H-2402 had only minor uses and consequently is abundant at mole fractions of 1 order of magnitude less than the other two halons. Its peak mole fraction was 0.50 ppt in the Northern Hemisphere in the early 2000s, and the global mean mole fraction has since declined to 0.42 ppt in 2015. Pollution events are limited to three events at most at each station's Medusa-GCMS record except for Gosan, where pollution events were detected frequently. Pollution events were also absent from Medusa-GCMS measurement records, which are otherwise not discussed further here. These records are from the "urban" sites in La Jolla (California, USA), Aspendale (Victoria, Australia), and Dubendorf (Zurich, Switzerland) that utilize laboratory-based instruments set to measure ambient air when not used for further purposes (unpublished data provided by SIO, CSIRO, and Empa, respectively). Additionally, no H-2402 pollution events were detected at the regional site at Tacolneston (Norfolk, England; unpublished data provided by the Universities of Bristol and East Anglia).

To further investigate the pronounced pollution events at Gosan, we have conducted a footprint analysis based on FLEXPART (see section 2.9.4), which we combined with our observations. This revealed areas that
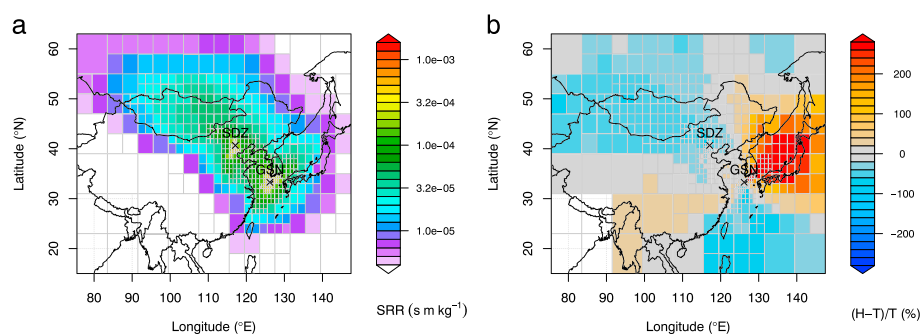
Figure 6. (a) Total footprint, T, for the H-2402 observations at the sites Gosan (GSN) and Shangdianzi (SDZ) for the period 1 January 2010 to 31 December 2014, given as source-receptor relationship (SRR) in units s m kg^{-1}. (b) Difference between average polluted footprint (H) and the average overall footprint (T), normalized by T, based on measurements from both stations. The polluted footprint represents those situations when the H-2402 observations were 0.02 ppt larger than the estimated baseline mole fraction. Note that the footprint was calculated on an irregular grid with the smallest grid boxes close to the sites and large grid boxes away from the site where overall source sensitivities were small. In empty grid boxes source sensitivities were zero.

are connected with increased levels of H-2402 (Figure 6). The analysis shows that the highest concentrations of H-2402 as observed at Gosan were connected with air masses arriving from the northeast. The potential source area covers mainly the Sea of Japan/East Sea and the adjacent countries with higher emissions nearer Japan. It appears possible that the observed emissions stem from H-2402 sources of the Russian Federation, which is the largest user of H-2402 [*HTOC*, 2011, 2014c; *Kopylov et al.*, 2003]. However, source sensitivities were relatively low over the Russian Federation and this conclusion needs to be drawn with caution.

3.1.4. Equivalent Effective Stratospheric Chlorine

The three halons are powerful ozone-depleting substances (ODSs) primarily because they contain bromine, which is, on a per-molecule base, significantly more effective at destroying stratospheric ozone than chlorine [*Carpenter and Reimann*, 2014]. In order to quantitatively compare the three halons for their capacity to destroy ozone and to relate them to other ODSs, we use the parametrization of equivalent effective stratospheric chlorine (EESC). EESC, first introduced by *Daniel et al.* [1995], is a useful tool in interpreting stratospheric ozone changes at polar and midlatitudes. It uses fractional release factors, which represent the extent to which an ODS has photolyzed and released its reactive halogen in the stratosphere. These factors are dependent on compound and the amount of time an air mass has spent in the stratosphere. We use fractional release factors of 0.997 for H-1211, 0.798 for H-1301, and 0.999 for H-2402 for a transport time of 5.5 years from the troposphere to the stratosphere [*Newman et al.*, 2007]. To account for the above mentioned larger effectiveness of bromine to destroy stratospheric ozone compared to chlorine, EESC also uses the concept of an α factor to convert the bromine content of the halons to "equivalent chlorine." This α factor is here chosen as 65 [*Carpenter and Reimann*, 2014] for a transport time of 5.5 years from the troposphere to the polar stratosphere [*Newman et al.*, 2007]. For ozone changes at midlatitudes a transport time of ~3 years should be used. The resulting records of EESC are shown in Figure 7. In analogy to their mole fractions, the EESC for H-1211 and H-2402 is declining, while that of H-1301 is increasing. The projected EESC for the end of the record (2015 + 5.5 years) is 0.23 ppb (parts per billion, 10^{-9}), 0.16 ppb, and 0.050 ppb for the three compounds, respectively. The tropospheric measurements through the end of 2015 suggest that the combined EESC from the three halons peaked in the polar stratosphere in 2009–2012 at 0.47 ppb and will decrease to 0.44 ppb by 2020. A further decline in the stratosphere after 2020 is expected because the combined decrease of EESC from H-1211 and H-2402 is likely to continue to remain larger than the current small increase in EESC from H-1301. The collective EESC for the three halons has also been declining from 0.47 ppb ~8 years before the end of the record to ~0.44 ppb, and it is expected to further decline because the combined decrease of the atmospheric abundances of H-1211 and H-2402 is larger than the increase from H-1301. The fraction of the combined halon EESC to the total for all major known ODSs (excluding nitrous oxide) has grown over time from an insignificant fraction in the 1970s to a contribution of ~13% of the total EESC (3.5 ppb) at the end of the record (2015 + 5.5 years). This is also illustrated in Figure 7 and reported in *Fraser et al.* [2014] and at http://www.esrl.noaa.gov/gmd/odgi/.
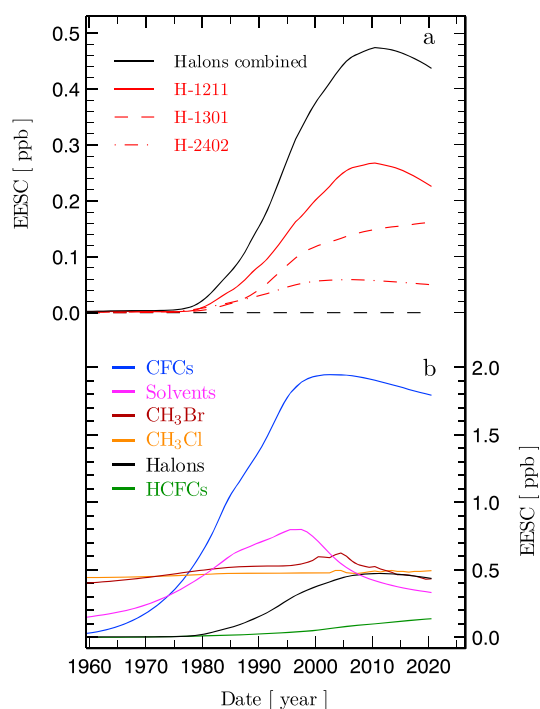
Figure 7. Contribution to equivalent effective stratospheric chlorine (EESC) for the halons H-1211 (CBrClF$_2$), H-1301 (CBrF$_3$), and H-2402 (CBrF$_2$CBrF$_2$). (a) Halon contributions are based on this work, and those of (b) all major EESC contributors are based on AGAGE data (unpublished). CFCs: chlorofluorocarbons are the sum of CFC-11, CFC-12, CFC-113, CFC-114, and CFC-115. HCFCs: hydrochlorofluorocarbons are the sum of HCFC-22, HCFC-141b, and HCFC-142b. Solvents are CHCBrF$_3$CClCBrF$_3$ and CCl$_4$. Calculations are based on the assumption of Br being 65 times more effective in ozone destruction than chlorine (α factor) and using fractional release factors of 0.997, 0.798, and 0.999 for the three compounds, respectively [*Newman et al.*, 2007]. The calculations are based on a time lag for air mass transport to the polar stratosphere of 5.5 years resulting in EESCs up to the year 2020.5. Age spectrum influences were not included in the results shown here.

For completeness it is important to mention that the halons also contribute significantly to the bromine loading of the stratosphere. This is discussed in detail in the latest WMO/UNEP report [*Carpenter and Reimann*, 2014] and has shown that the contribution of stratospheric bromine derived from these three halons is nearly half of the total bromine if all anthropogenic and natural bromine sources are accounted for (including very short lived bromine compounds). The present halon results do not significantly change the findings of that WMO/UNEP report.

3.2. Top-Down Emissions

We calculate global observation-based (top-down) emissions of the halons using the two inversion approaches described in section 2.9.3. The results are shown in Figure 8 and tabulated in the supporting information. Both inversion methods were applied to the combined AGAGE record, which consists of the firn and canister-archived air measurements, the AGAGE and Monte Cimone in situ, and the King Sejong flask sample measurements (all on the SIO calibration scales). Emissions were also separately calculated based on the NOAA network data but using the "Bristol inversion" only. The results for each network shown in Figure 8 were calculated and reported on the respective calibration scales, i.e., data were not converted onto a common scale to keep the data sets independent. The total uncertainties are also shown in Figure 8. They are dominated by the uncertainties in the lifetimes of the halons. Emissions before 1960 were found to be absent within the uncertainties of the calculations and are hence omitted from figures and tables.

The emissions (based on AGAGE observations) for all three halons peaked approximately two decades ago and have since been steadily declining. There are surprising differences in the timing of their peak emissions; H-2402 and H-1301 emissions peaked earlier (~1989) compared to H-1211 (1995–1998). While the decline in the emissions of H-1211 and H-2402 has been more gradual, those of H-1301 declined relatively rapidly after their peak. The largest emissions are estimated for H-1211 peaking at ~11 kt yr^{-1} followed by
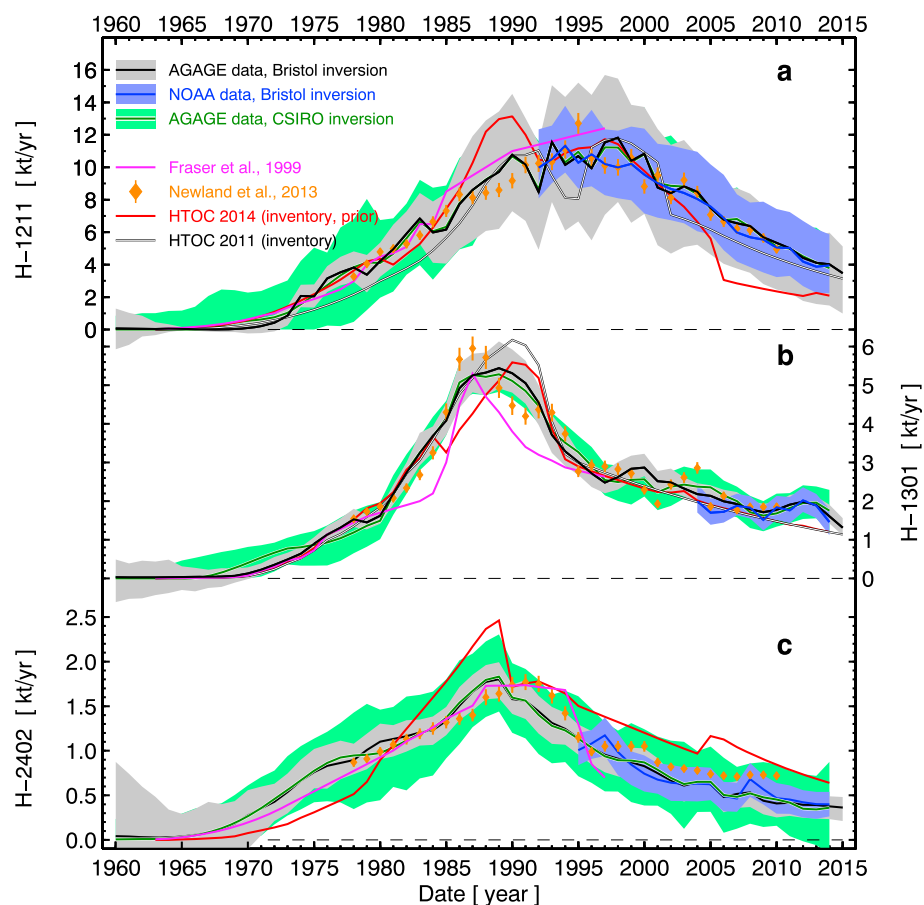
Figure 8. Global emissions (kt yr^{-1}) to the atmosphere of the halons (a) H-1211, (b) H-1301, and (c) H-2402 derived from atmospheric observations and production-based inventories. The emissions calculated in this study from the Bristol inversion are given as black solid lines for the AGAGE data with the uncertainties (1σ) as gray bands and those for the NOAA data as dark blue lines and light blue bands, respectively. The emissions calculated from the CSIRO inversion (AGAGE data) are given in green with the respective (1σ) uncertainty bands in light green. These emissions are compared to the observation-based emission estimated by *Fraser et al.* [1999] (magenta line) and *Newland et al.* [2013] (light orange diamonds), both derived from the Cape Grim Air Archive data set. The bottom-up inventory-based emission estimates by the Halon Technical Options Committee (HTOC) using the 2010 [*HTOC*, 2011] and 2014 [*HTOC*, 2014a] (numerical data unpublished) estimates are shown as white and red solid lines, respectively.

those of H-1301 at ~5.4 kt yr^{-1}, while the H-2402 emissions were at ~1.8 kt yr^{-1}. By the end of the record (mean of 2013–2015) they have declined to 3.9 kt yr^{-1} for H-1211, 1.6 kt yr^{-1} for H-1301, and 0.38 kt yr^{-1} for H-2402.

The uncertainties in the emissions of H-1301 are considerably smaller than those of H-1211 and H-2402. This is caused not only by the smaller uncertainty in the H-1301 lifetime but also by its longer lifetime (Table 1). For a compound with longer lifetime, a change in emissions in a particular year will influence the atmospheric abundance (observations) for a longer period. Therefore, there are effectively more observations constraining the emissions in any particular year for H-1301, compared to the other species, and consequently, the uncertainties are reduced.

The Bristol and CSIRO inversion results agree well for the most part with some minor discrepancies for H-1301, which, however, did not show a systematic offset (Figure 8). The Bristol inversion was run for the AGAGE and NOAA data independently. The derived emissions agree well for the overlapping period (Figure 8) despite the small differences in calibration scales.

In Figure 8 we also compare our Bristol emission results based on the AGAGE data with the emissions derived by *Fraser et al.* [1999] and *Newland et al.* [2013], which are both derived solely from the CGAA. Our calculated emissions agree within the uncertainties for the most part of the overlapping periods with these earlier
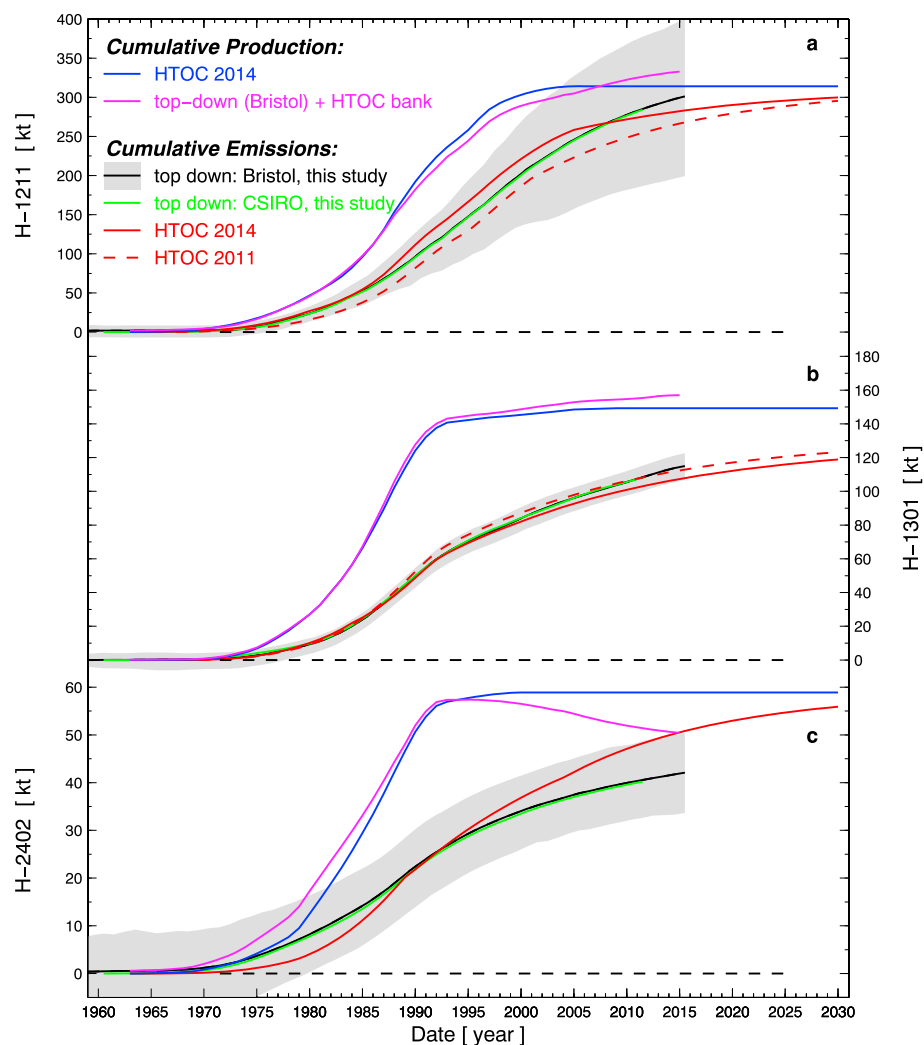
Figure 9. Global cumulative (in time) emissions and productions of the halons (a) H-1211, (b) H-1301, and (c) H-2402. Our observation-based top-down emissions are based on the AGAGE data (black line for Bristol inversion with gray uncertainty bands and green line for CSIRO inversion). These cumulative emissions are compared to the global inventory-based bottom-up cumulative emissions (red solid lines) from the HTOC 2014 assessment [*HTOC*, 2014a] (unpublished data) and the *HTOC* [2011] estimates. The sums of our top-down cumulative emissions estimates and the HTOC 2014 banks are shown as magenta solid lines and compared to the global cumulative production estimates (blue lines).

results. However, the three emission estimates are based on lifetimes and calibration scales, which in some cases differ significantly from one another, and hence, a conversion to common lifetimes and calibration scales could potentially lead to significantly altered differences between these studies. For H-1301 we find that the peak emissions in the records by *Fraser et al.* [1999] and *Newland et al.* [2013] are advanced by several years compared to our estimates, while for H-2402 they are delayed.

Our observation-based top-down emission estimates are also compared with the two latest HTOC bottom-up inventory-based estimates (Figure 8). It is noteworthy to emphasize that the HTOC estimates are made independently of any previous results derived from atmospheric observations. For H-1211 there are some considerable differences between our best estimates and the HTOC 2014 estimates with ours being lower in the late 1980s but higher for the last decade. This latest difference has become more pronounced with the update from HTOC 2011 to HTOC 2014. For H-1301, the bottom-up estimates agree reasonably well with our best estimates but reveal a persistent difference over the last years when our estimates are higher. For H-2402, our best estimate emissions are higher compared to the HTOC 2014 estimates until ~1980 and lower for most of the remaining record. These comparisons only apply to our best estimates of emissions. If we take
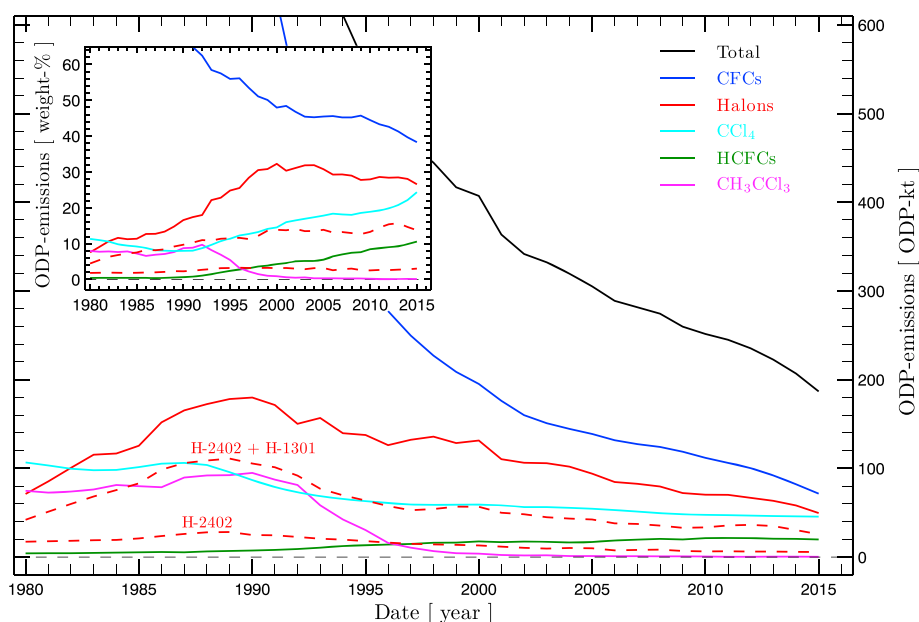
Figure 10. Annual global emissions of the halons H-1211, H-1301, and H-2402, weighted by ozone depletion potential (ODP). ODP values from WMO 2014 [*Harris et al.*, 2014] (see Table 1) were used in these calculations. The total of the three halons is shown as a red solid line with separations for the cumulatively stacked H-2402, H-1301, and H-1211 from bottom to top (dashed red lines). The insert shows the halon contribution as percentage to all major ozone-depleting substances (ODSs), excluding nitrous oxide. Cumulative stacking of the halons is the same as in the main panel, but the individual halon contributions are not part of the 100%. Emissions of halons is from this work, all other emissions are based on *Rigby et al.* [2014] with extensions to 2015. Here CFCs are the sum of CFC-11, CFC-12, CFC-13, CFC-113, CFC-114, and CFC-115; HCFCs are the sum of HCFC-22, HCFC-124, HCFC-141b, and HCFC-142b. ODP values are also from *Harris et al.* [2014] except for CFC-13 (for which a value of 1 was chosen).

into account the uncertainties in our estimates, and assuming similarly large uncertainties in the bottom-up estimates, then the results derived by the two approaches agree with each other.

We also compare cumulative emissions (Bristol inversion) with *HTOC* [2014a] total production and banks (Figure 9). The H-1211 cumulative emissions up to and including 2015, which we derive using the top-down approach, are 301 (200–400) kt and slightly exceed the cumulative emissions derived from the HTOC 2014 data. If we added to these emissions the estimated banked H-1211 of 32 kt [*HTOC*, 2014a], then a total global production results, which slightly exceeds that of 314 kt estimated by HTOC [*HTOC*, 2014a] for 2015. These estimates currently agree within the large uncertainties of our estimated cumulative emissions and the presumably large uncertainties in the HTOC estimates (uncertainties in the *HTOC* [2014a] production and banks are not available). However, there are indications of significant expected future emissions, which will increase the apparent discrepancy between our observation-based top-down cumulative emissions and the total production. Our estimates show high ongoing emissions (Figure 8) at ~4 kt yr^{-1}, which are still nearly one third of the peak emissions of the 1990s (Figure 8). Also, these emissions are declining relatively slowly, in particular when compared to, e.g., the CFC emissions [*Carpenter and Reimann*, 2014]. This is surprising given that enhanced efforts are expected to be in place to prevent H-1211 release from installed equipment as this compound is still in high demand and availability through recycling is becoming more difficult. Destruction of H-1211, which is not included in the above consideration, is believed to be small (<0.5 kt total for H-1211) (D. Verdonik, personal communication, 2015).

For H-1301 our cumulative emissions are 115 (106–123) kt, which is in good agreement with the *HTOC* [2014a] cumulative emissions or, equivalently, with the estimates of a total production of 149 kt and a remaining 2015 bank of 42 kt (Figure 9). For this compound the current emissions persist at ~1.6 kt yr^{-1}, which is about one third of the peak emissions in the 1990s. The lingering emissions of H-1301 over the next decades may well account for the HTOC 2015 bank estimate, suggesting that our results agree much better with the production estimates compared to H-1211. The uncertainties in these cumulative emissions are

smaller than those for H-1211 because of the longer lifetime and its smaller uncertainty, as already mentioned earlier. This large remaining bank for H-1301 (~30% of the production) and the lingering significant emissions imply that the global atmospheric H-1301 mole fraction is likely to not significantly decrease over the next decades.

Our derived cumulative emissions of H-2402 in 2015 are 42 (34–50) kt, which compares with *HTOC* [2014a] cumulative emissions of 51 kt, while the total production is estimated at 59 kt hence yielding a remaining bank of 8 kt (Figure 9). While our best estimate cumulative emissions for H-2402 were slightly larger than those by HTOC in the earlier part of the record, they are considerably smaller by 2015 indicating that the total production may be overestimated.

In order to compare the contribution to stratospheric ozone depletion of each halon with other ODSs and between each halon species, we calculate ODP emissions by multiplying the kiloton emissions (Bristol inversion) with respective ODP (ODP values from the WMO Ozone Assessment 2014 [*Harris et al.*, 2014] are used here). The summed halon ODP emissions for all three halons peaked at 180 ODP kt in 1990 and have since declined to 50 ODP kt in 2015 with 24 ODP kt, 20 ODP kt, and 5.7 ODP kt for H-1211, H-1301, and H-2402, respectively (Figure 10). Over the past decades, ODP-weighted emissions of halons have declined at smaller rates compared to emissions of the other potent anthropogenic ODSs. As a consequence, the halon ODP-weighted halon emission contribution relative to all major anthropogenic ODSs (CFCs, HCFCs, CHCBrF$_3$CClCBrF$_3$, CCl$_4$, excluding nitrous oxide) has increased from ~10% in the 1980s to ~30% (by ODP weight) in 1998 and since remained at this high percentage.

4. Conclusions

We present global long-term observations and derived observation-based top-down emissions for the three major halons. Globally averaged atmospheric abundances have been declining for H-1211 since 2005 and for H-2402 since the early 2000s. In contrast, abundances for H-1301 are still increasing. Global emissions, which we derive from observations, are robust and show similar trends and magnitudes independent of measurement program or analysis technique. The emissions have declined for all three halons, for H-1211 since the late 1990s, for H-1301 since ~1990, and for H-2402 since the late 1980s. However, for H-1211 and H-1301, the declines in emissions are slower than those reported by the HTOC, while those for H-2402 are faster. Although currently within the large uncertainties of the estimates, there are apparent discrepancies between our cumulative H-1211 and H-2402 emissions when compared to the respective total global production and current banks as estimated by HTOC [*HTOC*, 2014a].

References

Ashbaugh, L. L., W. C. Malm, and W. Z. Sadeh (1985), A residence time probability analysis of sulfur concentrations at Grand Canyon National Nark, *Atmos. Environ.*, *19*(8), 1263–1270, doi:10.1016/0004-6981(85)90256-2.

Bernard, F., M. R. McGillen, E. L. Fleming, C. H. Jackman, and J. B. Burkholder (2015), CBrF$_3$ (Halon-1301): UV absorption spectrum between 210 and 320 K, atmospheric lifetime, and ozone depletion potential, *J. Photochem. Photobiol. A*, *306*, 13–20, doi:10.1016/j.jphotochem.2015.03.012.

Buizert, C., et al. (2012), Gas transport in firn: Multiple-tracer characterisation and model intercomparison for NEEM, Northern Greenland, *Atmos. Chem. Phys.*, *12*, 4259–4277, doi:10.5194/acp-12-4259-2012.

Burkholder, J. B., R. R. Wilson, T. Gierczak, R. Talukdar, S. A. McKeen, J. L. Orlando, G. L. Vaghjiani, and A. R. Ravishankara (1991), Atmospheric fate of CBrF$_3$, CBr$_2$F$_2$, CBrClF$_2$, and CBrF$_2$CBrF$_2$, *J. Geophys. Res.*, *96*(D3), 5025–5043, doi:10.1029/90JD02735.

Butler, J. H., J. W. Elkins, B. D. Hall, S. O. Cummings, and S. A. Montzka (1992), A decrease in the growth rates of atmospheric halon concentrations, *Nature*, *359*(6394), 403–405, doi:10.1038/359403a0.

Butler, J. H., S. A. Montzka, A. D. Clarke, J. M. Lobert, and J. W. Elkins (1998), Growth and distribution of halons in the atmosphere, *J. Geophys. Res.*, *103*(D1), 1503–1511, doi:10.1029/97JD02853.

Butler, J. H., M. Battle, M. L. Bender, S. A. Montzka, A. D. Clarke, E. S. Saltzman, C. M. Sucher, J. P. Severinghaus, and J. W. Elkins (1999), A record of atmospheric halocarbons during the twentieth century from polar firn air, *Nature*, *399*(6738), 749–755, doi:10.1038/21586.

Butler, J. H., S. A. Montzka, M. Battle, A. D. Clarke, D. J. Mondeel, J. A. Lind, B. D. Hall, and J. W. Elkins (2001), Collection and analysis of firn air from the South Pole, *Abstract #A51F-0145 presented at 2001 Fall Meeting*, AGU, San Francisco, Calif., 10–14 Dec.

Carpenter, L. J., S. Reimann, J. B. Burkholder, C. Clerbaux, B. D. Hall, R. Hossaini, J. C. Laube, and S. A. Yvon-Lewis (2014), Ozone-depleting substances (ODSs) and other gases of interest to the Montreal Protocol, Chapter 1, in *Scientific Assessment of Ozone Depletion: 2014, Global Ozone Research and Monitoring Project — Report No. 55*, vol. 55, World Meteorological Organisation, Geneva, Switz.

Clerbaux, C., et al. (2007), Long-lived compounds, Chapter 1, in *Scientific Assessment of Ozone Depletion: 2006, Global Ozone Research and Monitoring Project-Report No. 50*, p. 572, World Meteor. Or., Geneva, Switz.

Cunnold, D. M., R. F. Weiss, R. G. Prinn, D. Hartley, P. G. Simmonds, P. J. Fraser, B. Miller, F. N. Alyea, and L. Porter (1997), GAGE/AGAGE measurements indicating reductions in global emissions of CCl$_3$F and CCl$_2$F in 1992-1994, *J. Geophys. Res.*, *102*(D1), 1259–1269, doi:10.1029/96JD02973.

Cunnold, D. M., R. G. Prinn, R. A. Rasmussen, P. G. Simmonds, F. N. Alyea, C. A. Cardelino, A. J. Crawford, P. J. Fraser, and R. D. Rosen (1983), The Atmospheric Lifetime Experiment 3. Lifetime methodology and application to three years of $CFCl_3$ data, *J. Geophys. Res.*, *88*(NC13), 8379–8400, doi:10.1029/JC088iC13p08379.

Cunnold, D. M., et al. (2002), In situ measurements of atmospheric methane at GAGE/AGAGE sites during 1985–2000 and resulting source inferences, *J. Geophys. Res.*, *107*(D14), 4225, doi:10.1029/2001JD001226.

Daniel, J. S., S. Solomon, and D. L. Albritton (1995), On the evaluation of halocarbon radiative forcing and global warming potentials, *J. Geophys. Res.*, *100*(D1), 1271–1285, doi:10.1029/94JD02516.

Fraser, P. J., D. E. Oram, C. E. Reeves, S. A. Penkett, and A. McCulloch (1999), Southern Hemispheric halon trends (1978–1998) and global halon emissions, *J. Geophys. Res.*, *104*(D13), 15,985–15,999, doi:10.1029/1999JD900113.

Fraser, P. J., et al. (2014), Equivalent effective stratospheric chlorine from Cape Grim air archive, Antarctic firn, and AGAGE global measurements of ozone depleting substances, in *Baseline Atmospheric Program (Australia) 2009–2010*, pp. 17–23.

Hall, B. D., et al. (2014), Results from the International Halocarbon in Air Comparison Experiment (IHALACE), *Atmos. Meas. Tech.*, *7*, 469–490, doi:10.5194/amt-7-469-2014.

Harris, N. R. P., D. J. Wuebbles, J. S. Daniel, J. Hu, L. J. M. Kuijpers, K. S. Law, M. J. Prather, and R. Schofield (2014), Scenarios and information for policymakers, Chapter 5, in *Scientific Assessment of Ozone Depletion: 2014, Global Ozone Research and Monitoring Project—Report No. 55*, vol. 55, World Meteorol. Org., Geneva, Switz.

Hofmann, D. J., and S. A. Montzka (2009), Recovery of the ozone layer, *Eos Trans. AGU*, *90*(1).

HTOC (2007), *2006 Assessment Report of the Halons Technical Option Committee*, United Nations Environment Programme Ozone Secretariat, 154 pp., Nairobi, Kenya.

HTOC (2011), *2010 Assessment Report of the Halons Technical Option Committee*, United Nations Environment Programme Ozone Secretariat, 149 pp., Nairobi, Kenya.

HTOC (2014a), 2014 Assessment Report, in *UNEP Report of the Halons Technical Options Committee*, vol. 1, p. 30, United Nations Environment Programme Ozone Secretariat, Nairobi, Kenya.

HTOC (2014b), 2014 Supplementary Report #1; Civil Aviation, in *UNEP Report of the Halons Technical Options Committee*, vol. 2, p. 12, United Nations Environment Programme Ozone Secretariat, Nairobi, Kenya.

HTOC (2014c), 2014 Supplementary Report #2; Global Halon 1211, 1301, and, 2402 Banking, in *UNEP Report of the Halons Technical Options Committee*, vol. 3, p. 31, United Nations Environment Programme Ozone Secretariat, Nairobi, Kenya.

Ivy, D. J., et al. (2012), Atmospheric histories and growth trends of C_4F_{10}, C_5F_{12}, C_6F_{14}, C_7F_{16} and C_8F_{18}, *Atmos. Chem. Phys.*, *12*, 4313–4325, doi:10.5194/acp-12-4313-2012.

Kopylov, N. P., V. M. Nikolayev, A. F. Zhevlakov, V. V. Pivovarov, and V. N. Tselikov (2003), *Russian National Strategy for Halon Management*, Chimizdat, 40 pp., St. Petersburg, Moscow.

Langenfelds, R. L., P. J. Fraser, R. J. Francey, L. P. Steele, L. W. Porter, and C. E. Allison (1996), The Cape Grim air archive: The first seventeen years, 1978–1995, in *Baseline Atmospheric Program (Australia) 1994–95*, edited by R. J. Francey, A. L. Dick, and N. Derek, pp. 53–70, Bureau of Meteorol. and CSIRO Division of Atmos. Res., Australian Bureau of Meteorol. and CSIRO Marine and Atmos. Res., Melbourne, Australia.

Langenfelds, R. L., P. B. Krummel, P. J. Fraser, L. P. Steele, J. Ward, and N. T. Somerville (2014), Archiving of Cape Grim air, in *Baseline Atmospheric Program Australia 2009–2010*, edited by N. Derek, P. B. Krummel, and S. J. Cleland, pp. 44–45, Australian Bureau of Meteorol. and CSIRO Marine and Atmos. Res., Melbourne, Australia.

Laube, J. C., A. Keil, H. Bönisch, A. Engel, T. Röckmann, C. M. Volk, and W. T. Sturges (2013), Observation-based assessment of stratospheric fractional release, lifetimes, and ozone depletion potentials of ten important source gases, *Atmos. Chem. Phys.*, *13*, 2779–2791, doi:10.5194/acp-13-2779-2013.

Maione, M., U. Giostra, J. Arduini, F. Furlani, F. Graziosi, E. Lo Vullo, and P. Bonasoni (2013), Ten years of continuous observations of stratospheric ozone depleting gases at Monte Cimone (Italy)—Comments on the effectiveness of the Montreal Protocol from a regional perspective, *Sci. Tot. Environ.*, *155–164*, 445–446, doi:10.1016/j.scitotenv.2012.12.056.

McCulloch, A. (1992), Global production and emissions of bromochlorodifluoromethane and bromotrifluoromethane (halon-1211 and halon-1301), *Atmos. Environ.*, *26A*(7), 1325–1329, doi:10.1016/0960-1686(92)90392-X.

Miller, B. R., R. F. Weiss, P. K. Salameh, T. Tanhua, B. R. Greally, J. Mühle, and P. G. Simmonds (2008), Medusa: A sample preconcentration and GC/MS detector system for in situ measurements of atmospheric trace halocarbons, hydrocarbons, and sulfur compounds, *Anal. Chem.*, *80*(5), 1536–1545, doi:10.1021/ac702084k.

Montzka, S. A., et al. (2011), Ozone-depleting substances (ODSs) and related chemicals, Chapter 1, in *Scientific Assessment of Ozone Depletion: 2010, Global Ozone Research and Monitoring Project—Report No. 52*, World Meteorological Organisation, Geneva, Switz.

Montzka, S. A., R. C. Myers, J. H. Butler, and J. W. Elkins (1993), Global tropospheric distribution and calibration scale of HCFC-22, *Geophys. Res. Lett.*, *20*(8), 703–706, doi:10.1029/93GL00753.

Montzka, S. A., J. H. Butler, B. D. Hall, J. W. Elkins, and D. J. Mondeel (2003), A decline in tropospheric organic bromine, *Geophys. Res. Lett.*, *30*(15), 1826, doi:10.1029/2003GL017745.

Mühle, J., et al. (2010), Perfluorocarbons in the global atmosphere: Tetrafluoromethane, hexafluoroethane, and octafluoropropane, *Atmos. Chem. Phys.*, *10*, 5145–5164, doi:10.5194/acp-10-5145-2010.

Myhre, G., et al. (2013), Anthropogenic and natural radiative forcing, in *Climate Change 2013: The Physical Science Basis. Contribution of Working Group I to the Fifth Assessment Report of the Intergovernmental Panel on Climate Change*, edited by T. F. Stocker et al., Cambridge Univ. Press, Cambridge, U. K., and New York.

Newland, M. J., C. E. Reeves, D. E. Oram, J. C. Laube, W. T. Sturges, C. Hogan, P. Begley, and P. J. Fraser (2013), Southern hemispheric halon trends and global halon emissions, 1978–2011, *Atmos. Chem. Phys.*, *13*, 5551–5565, doi:10.5194/acp-13-5551-2013.

Newman, P. A., J. S. Daniel, D. W. Waugh, and E. R. Nash (2007), A new formulation of equivalent effective stratospheric chlorine (EESC), *Atmos. Chem. Phys.*, *7*, 4537–4552, doi:10.5194/acp-7-4537-2007.

O'Doherty, S., et al. (2001), In situ chloroform measurements at Advanced Global Atmospheric Gases Experiment atmospheric research stations from 1994 to 1998, *J. Geophys. Res.*, *106*(D17), 20,429–20,444, doi:10.1029/2000JD900792.

O'Doherty, S., et al. (2014), Global emissions of HFC-143a (CH_3CF_3) and HFC-32 (CH_2F_2) from in situ and air archive atmospheric observations, *Atmos. Chem. Phys.*, *14*, 9249–9258, doi:10.5194/acp-14-9249-2014.

Papanastasiou, D. K., N. R. Carlon, J. A. Neuman, E. L. Fleming, C. H. Jackman, and J. B. Burkholder (2013), Revised UV absorption spectra, ozone depletion potentials, and global warming potentials for the ozone-depleting substances CF_2Br_2, CF_2ClBr, and CF_2BrCF_2Br, *Geophys. Res. Lett.*, *40*(2), 464–469, doi:10.1002/grl.50121.

Prinn, R. G., et al. (2000), A history of chemically and radiatively important gases in air deduced from ALE/GAGE/AGAGE, *J. Geophys. Res.*, *105*, 17,751–17,792, doi:10.1029/2000JD900141.

Reeves, C. E., W. T. Sturges, G. A. Sturrock, K. Preston, D. E. Oram, J. Schwander, R. Mulvaney, J.-M. Barnola, and J. Chappellaz (2005), Trends of halon gases in polar firn air: Implications for their emission distributions, *Atmos. Chem. Phys.*, *5*, 2055–2064, doi:10.5194/acp-5-2055-2005.

Rigby, M., et al. (2010), History of atmospheric SF$_6$ from 1973–2008, *Atmos. Chem. Phys.*, *10*, 10,305–10,320, doi:10.5194/acp-10-10305-2010.

Rigby, M., A. L. Ganesan, and R. G. Prinn (2011), Deriving emissions from sparse mole-fraction time series, *J. Geophys. Res.*, *116*, D08306, doi:10.1029/2010JD015401.

Rigby, M., et al. (2013), Re-evaluation of lifetimes of the major CFCs and CH$_3$CCl$_3$ using atmospheric trends, *Atmos. Chem. Phys.*, *13*, 2691–2702, doi:10.5194/acp-13-2691-2013.

Rigby, M., et al. (2014), Recent and future trends in synthetic greenhouse gas radiative forcing, *Geophys. Res. Lett.*, *41*, 2623–2630, doi:10.1002/2013GL059099.

Rommelaere, V., L. Arnaud, and J.-M. Barnola (1997), Reconstructing recent atmospheric trace gas concentrations from polar firn and bubbly ice data by inverse methods, *J. Geophys. Res.*, *102*(D25), 30,069–30,083, doi:10.1029/97JD02653.

Ruckstuhl, A. F., S. Henne, S. Reimann, M. Steinbacher, M. K. Vollmer, S. O'Doherty, B. Buchmann, and C. Hueglin (2012), Robust extraction of baseline signal of atmospheric trace species using local regression, *Atmos. Meas. Tech.*, *5*, 2613–2624, doi:10.5194/amt-5-2613-2012.

Schwander, J., J. M. Barnola, C. Andrié, M. Leuenberger, A. Ludin, D. Raynaud, and B. Stauffer (1993), The age of the air in the firn and the ice at Summit, Greenland, *J. Geophys. Res.*, *98*(D2), 2831–2838, doi:10.1029/92JD02383.

Seibert, P., and A. Frank (2004), Source-receptor matrix calculation with a Lagrangian particle dispersion model in backward mode, *Atmos. Chem. Phys.*, *4*, 51–63, doi:10.5194/acp-4-51-2004.

Simmonds, P. G., S. O'Doherty, G. Nickless, G. A. Sturrock, R. Swaby, P. Knight, J. Ricketts, G. Woffendin, and R. Smith (1995), Automated gas chromatograph mass spectrometer for routine atmospheric field measurements of the CFC replacement compounds, the hydrofluorocarbons and hydrochlorofluorocarbons, *Anal. Chem.*, *67*(4), 717–723, doi:10.1021/ac00100a005.

SPARC (2013), SPARC report on the lifetimes of stratospheric ozone-depleting substances, their replacements, and related species, *Tech. Rep.* 6, WCRP-15/2013. [Available at http://www.sparc-climate.org/publications/sparc-reports/sparc-report-no6/.]

Spivakovsky, C. M., et al. (2000), Three-dimensional climatological distribution of tropospheric OH: Update and evaluation, *J. Geophys. Res.*, *105*(D7), 8931–8980.

Stohl, A., C. Forster, A. Frank, P. Seibert, and G. Wotawa (2005), Technical note: The Lagrangian particle dispersion model FLEXPART version 6.2, *Atmos. Chem. Phys.*, *5*, 2461–2474, doi:10.5194/acp-5-2461-2005.

Sturrock, G. A., D. M. Etheridge, C. M. Trudinger, P. J. Fraser, and A. M. Smith (2002), Atmospheric histories of halocarbons from analysis of Antarctic firn air: Major Montreal Protocol species, *J. Geophys. Res.*, *107*(D24), 4765, doi:10.1029/2002JD002548.

Trudinger, C. M., I. G. Enting, D. M. Etheridge, R. J. Francey, V. A. Levchenko, L. P. Steele, D. Raynaud, and L. Arnaud (1997), Modeling air movement and bubble trapping in firn, *J. Geophys. Res.*, *102*(D6), 6747–6763, doi:10.1029/96JD03382.

Trudinger, C. M., D. M. Etheridge, P. J. Rayner, I. G. Enting, G. A. Sturrock, and R. L. Langenfelds (2002), Reconstructing atmospheric histories from measurements of air composition in firn, *J. Geophys. Res.*, *107*(D24), 4780, doi:10.1029/2002JD002545.

Trudinger, C. M., I. G. Enting, P. J. Rayner, D. M. Etheridge, C. Buizert, M. Rubino, P. B. Krummel, and T. Blunier (2013), How well do different tracers constrain the firn diffusivity profile?, *Atmos. Chem. Phys.*, *13*, 1485–1510, doi:10.5194/acp-13-1485-2013.

Verdonik, D. P., and M. L. Robin (2004), Analysis of emission data, estimates, and modelin of fire protection agents, *Proceedings of the Earth Technology Forum*, 11 pp., Washington, D. C.

Vollmer, M. K., et al. (2011), Atmospheric histories and global emissions of the anthropogenic hydrofluorocarbons HFC-365mfc, HFC-245fa, HFC-227ea, and HFC-236fa, *J. Geophys. Res.*, *116*, D08304, doi:10.1029/2010JD015309.

Vollmer, M. K., T. S. Rhee, M. Rigby, D. Hofstetter, M. Hill, F. Schoenenberger, and S. Reimann (2015), Modern inhalation anesthetics: Potent greenhouse gases in the global atmosphere, *Geophys. Res. Lett.*, *42*, 1606–1611, doi:10.1002/2014GL062785.

Wamsley, P. R., et al. (1998), Distribution of halon-1211 in the upper troposphere and lower stratosphere and the 1994 total bromine budget, *J. Geophys. Res.*, *103*(D1), 1513–1526, doi:10.1029/97JD02466.